Sveriges lantbruksuniversitet
Swedish University of Agricultural Sciences

Department of Soil and Environment

Nanoplastic transport in soils by advection and bioturbation

Wiebke Mareile Heinze

Master's Thesis in Environmental Science
EnvEuro – European Master in Environmental Science Sciences

Examensarbeten, Institutionen för mark och miljö, SLU
2019:10

Uppsala 2019

Nanoplastic transport in soils by advection and bioturbation

Wiebke Mareile Heinze

Supervisor: Geert Cornelis, Department of Soil and Environment, SLU
Assistant supervisor: Bjarne W. Strobel, Department of Plant and Environmental Sciences, University of Copenhagen
Examiner: Nicholas Jarvis, Department of Soil and Environment, SLU

Credits: 30 ECTS
Level: Second cycle, A2E
Course title: Independent Project in Environmental Science – Master´s thesis
Course code: EX0897
Programme/Education: EnvEuro – European Master in Environmental Science 120 credits
Course coordinating department: Soil and Environment

Place of publication: Uppsala
Year of publication: 2019
Cover picture: photo by Wiebke Mareile Heinze
.
Title of series: Examensarbeten, Institutionen för mark och miljö, SLU
Number of part of series: 2019:10
Online publication: http://stud.epsilon.slu.se

Keywords: column leaching, attachment efficiency,exposure, mixing rates, modelling

Sveriges lantbruksuniversitet
Swedish University of Agricultural Sciences

Faculty of Natural Resources and Agricultural Sciences
Department of Soil and Environment

Abstract

Micro- and nanoplastics are increasingly perceived as an emerging threat to ecosystems. They are emitted to soils through different pathways, including sewage sludge or compost applications in agriculture, or through tire abrasion and degradation of mismanaged waste. Yet, their environmental behaviour and fate in terrestrial ecosystems is still poorly investigated. In order to investigate the potential impact of different transport processes on the redistribution of plastics in natural soils, column leaching tests and bioturbation studies in microcosms were conducted using a natural topsoil and palladium-doped polystyrene nanoplastics of 256 nm diameter. Under the influence of advection, nanoplastic retention in saturated columns was very limited. Kinetic transport parameters were obtained from saturated column tests by applying inverse modelling in HYDRUS-1D. Derived attachment efficiencies were relatively low, $\alpha_{att} = 6.25 \times 10^{-4}$. In unsaturated soils, more representative of prevailing field conditions, nanoplastic mobility through percolating water was very limited. However, the burrowing activity of anecic earthworms, here *Lumbricus terrestris*, caused a significant redistribution and transport of nanoplastics into deeper soil layers, steadily increasing over the duration of the experiment. Observed spatial and temporal changes in nanoplastic distribution were used to determine bioturbation rates by applying a bioturbation model ($k_{bioturb} = 4.5 \times 10^{-11}$). The bioturbation model systematically underestimated nanoplastics in the lower layers, indicating that further differentiation of the transport modes by soil biota might be necessary. Although mixing by earthworms was slow, the current study suggests that under field conditions bioturbation may be more important than advective transport for nanoplastics in soils. While displacement of nanoplastics likely reduces uptake and risks for terrestrial organisms and crops near the surface, potential effects in deeper soil layers are of yet unknown consequences. A wider array of nanoplastic types and sizes, as well as modes of applications is needed to allow for extrapolation of findings.

Popular scientific abstract

In the context of the steady increase of plastic consumption, microplastic pollution is becoming a growing concern of public authorities and individuals. Soils are often not considered in the public debates on plastic pollution. However, the emissions of micro- and nanoplastics to terrestrial ecosystems have recently been estimated to exceed the emissions to oceans by far. Microplastics enter soils mixed into sewage sludge and compost which is applied as fertilizer on land used for agricultural production. Even urban soils are exposed to small plastics from tire wear, artificial turfs and littering. The fate of these plastics after entering soils is currently unclear, as are associated potential risks, such as leaching to groundwaters, rivers and the marine ecosystems. In order to assess these risks, transport processes that may cause a redistribution of plastics in soils were investigated. This includes transport by water seeping through the soil. The specific nanoplastic type used in this study was very mobile when applied to very wet soil with artificial rainwater. Through data from leaching experiments it was possible to capture the observed dynamics in transport models. However, when soils were dry and water added only periodically, the same plastics were retained at the soil surface. In these cases, nanoplastics entering soils were still redistributed by the burrowing and mixing activity of earthworms. Although earthworms mix the soil relatively slowly, on the long-term considering historic and recent plastic emissions this transport process may cause substantial mixing of plastics into lower soil depths. In order to capture the transport dynamics by earthworms more accurately, the model needs further development. Environmental models are useful tools for predicting the behaviour of substances of concern, however for more widely applicable conclusions more plastic types and sizes have to be investigated.

Table of contents

Abbreviations

ARD	Advection-reaction-dispersion (equation)
BTC	breakthrough curve
CFT	Colloid filtration theory
DLVO	Derjaguin-Landau-Verwey-Overbeek
DOM	dissolved organic matter
ICP-MS	Inductively-coupled plasma – Mass spectrometer
In	indium
Pd	palladium
PE	polyethylene
PET	polyethylenterephthalat
PP	polypropylene
PS	polystyrene
PV	pore volume
PVC	polyvinylchloride

1 Introduction

Microplastic pollution of the environment is a growing concern. The presence of small plastic debris in freshwater, marine and even remote ecosystems has been reported, rapidly increasing public awareness (Auta et al., 2017; Avio et al., 2017; Bergmann et al., 2019). Global annual plastic production has risen to 330 million tonnes in 2016 and is expected to further increase in the future (Lebreton and Andrady, 2019; Singh and Sharma, 2016). Despite a recent increase in studies focussing on emissions of microplastics into the marine environment, there is still a considerable lack of knowledge on plastic concentrations and their fate in terrestrial ecosystems (Horton et al., 2017; Nizzetto et al., 2016; Rillig et al., 2017). Conversely, first material flow studies by Kawecki and Nowack (2019) estimate that plastic emissions to soils are exceeding emissions to marine systems by a factor of 40. In terms of microplastics, Horton et al. (2017) report approximately 473,000 to 910,000 tonnes to be released to the terrestrial environment within the EU annually. While generally treated as a sink, micro- and nanoplastics in soils constitute not only a potential hazard to terrestrial ecosystems but also a potential long-term source for freshwater and marine plastic pollution. Quantified estimates for actual abundance, interactions with soil constituents or organisms, mass transfers due to transport processes and associated leaching potential of microplastics are to-date poorly investigated (Bläsing and Amelung, 2018; Horton et al., 2017).

The major environmental concerns on plastic debris are associated with its persistence, the potential release of additives such as plasticizers, flame retardants or stabilizers with toxic or endocrine disrupting effects, and their uptake by organisms and potential trophic transfers (Andrady, 2017; Bläsing and Amelung, 2018; Horton et al., 2017). Micro- and nanoplastics are regarded as problematic in particular. Their higher surface area allows for more chemical interactions and sorption of persistent organic pollutants. Simultaneously, with decreasing size plastics can be taken up more easily by organisms through ingestion with potential adverse effects (Cauwenberghe et al., 2015). Previous studies on marine organisms found sub-lethal physical toxicity effects associated with ingestion of small plastics, affecting reproduction, growth and fitness (Cauwenberghe et al., 2015; von Moos et al., 2012). While research on the effects of microplastics on terrestrial organisms is still very fragmented, first studies indicate negative impact at high exposure concentrations (Huerta Lwanga et al., 2016; Nizzetto et al., 2016). For a complete risk assessment that can inform policy-making, it is necessary to substantiate the potential hazard of

micro- and nanoplastics with relevant environmental exposure levels (Muralikrishna and Manickam, 2017). As contaminants enter soils, different processes determine their environmental fate, i.e. whether accumulation occurs or whether substances are transferred to other environmental compartments. Different modes of transport may cause mass flows from the soil and changes in local concentrations, thereby determining whether soils act as sinks or become new sources. For soils, transport by percolating water, i.e. advection, is a widely acknowledged mechanism causing redistributions of particulate contaminants (Brusseau, 2019). Although often neglected, many studies have acknowledged the considerable contribution of bioturbation to the mixing of soils and hence it needs to be included in an integrated assessment of contaminant transport (Jarvis et al., 2010; Taylor et al., 2018). At present, knowledge on the dynamic of these transport processes and thus mass flows of microplastics in soils are poorly investigated (Bläsing and Amelung, 2018; Horton et al., 2017). A crucial step is to examine the suitability of existing fate models for predicting transport in soils and validate them using experimental data. To overcome general constraints in detecting plastic in environmental samples rich in organic carbon (Andrady, 2017; Bläsing and Amelung, 2018; Mitrano et al., 2019), the use of synthesized metal-doped plastics for process-studies has been proposed by Mitrano et al. (2019). Utilizing doped particles can provide first insights into the fate of plastic in the terrestrial environment and enable comparison between different modes of transport. Only with more in-depth knowledge about the fate of nanoplastics in soil is it possible to reliably estimate exposure levels of and implicated risks for terrestrial organisms, plants and, for urban soils, human health.

1.1 Aim of study

In order to provide useful transport parameters for estimating potential environmental exposure concentrations of terrestrial ecosystems and the fate of nanoplastics entering soils, the aim of this study was to investigate and quantify transport of nanoplastics in a natural soil through water movement and bioturbation, to derive transport parameters and investigate their suitability for predicting observed transport dynamics. This was achieved in four steps: 1) quantifying advection-driven transport of nanoplastics in column leaching tests with disturbed natural soil columns under saturated conditions, 2) using inverse modelling in HYDRUS-1D to derive particle-specific kinetic transport parameters, i.e. attachment efficiencies and detachment rates, 3) quantifying biologically mediated transport of nanoplastics by earthworms (*Lumbricus terrestis*) in a time-series of depth profiles and 4) deriving bioturbation rates for nanoplastics in the experimental setup. Obtained parameters were then assessed with regards to their suitability to predict observed nanoplastic mobility in soils. For both goals, suspensions of palladium-doped nanoplastics were utilized to overcome detection limitations. With first quantitative estimates of the two transport pathways established, and parameters that allow for comparison of observed dynamics with other studies, potential implications for nanoplastic pollution of soils were considered.

2 Theoretical background

2.1 Definitions of micro- and nanoplastics

The term microplastics is used to summarize a wide variety of polymers, primarily based on their size. For the specific terms and size boundaries to classify plastic particles however, there is still a considerable lack of consensus. Most current studies apply an upper limit of 5 mm to differentiate plastic micro- from mesodebris (Andrady, 2017; GESAMP, 2016; Horton et al., 2017). However, the included lower size-range differs substantially between authors and disciplines. Some authors include the complete nano-sized fraction in the term microplastic, while others suggest to draw a boundary between micro- and nanoplastics at 1 µm diameter (Horton et al., 2017). In the field of nanomaterial science the term nanoparticle is usually assigned to unbound or aggregated particles within the 1-100 nm range (2011/696/EU). As an alternative, Bläsing and Amelung (2018) propose the term colloidal plastics for particles of sizes 100-1000 nm. Due to the lack of a comprehensive classification, it is essential to clarify the terms on a study basis. In this study the term microplastics is employed to refer to plastic debris below 5 mm, and for simplicity the term nanoplastics is reserved for particles smaller than 1 µm.

Irrespective of size boundaries, the terms micro- and nanoplastics comprise a variety of polymers that differ in chemical composition and physical properties, such as specific density, crystallinity, polarity, colour or shape (Andrady, 2017). These polymers consist of long-chain molecular structures with repeated sequences of chemical units. Additives that are commonly used for enhancing specific properties are plasticizers, stabilizers, flame retardants and metals used for colouring (Andrady, 2017; GESAMP, 2016; Horton et al., 2017), the release of which is increasing with decreasing particle size. These additives add to the concern of plastic pollution, as many of these have shown to have toxic and endocrine-disrupting effects (Nizzetto et al., 2016; Oehlmann et al., 2009). Despite many differences, there are important characteristics that are shared among the material class of plastics, in particular hydrophobicity and a high resistance against degradation that is associated with their carbon backbone and high average molecular weight (Horton et al., 2017; Ng et al., 2018). Conversely, these are also major reasons for the environmental concern about micro- and nanoplastics and the need for investigating their environmental fate.

Plastics that are most extensively produced and thus most relevant for environmental assessments are polypropylene (PP), polyethylene (PE), polyethylene terephthalate (PET), polyvinylchloride (PVC) and polystyrene (PS) (Auta et al., 2017; GESAMP, 2015; Kawecki and Nowack, 2019). Correspondingly, these types are of primary interest for studies on micro- and nanoplastic fate in terrestrial systems.
A further distinction is often made into primary and secondary micro- and nanoplastics. Primary particles refers to industrially manufactured particles that are used in products, such as pellets, microbeads and powders, as additives in personal care products or industrial abrasives (Andrady, 2017; Horton et al., 2017; Rillig et al., 2017). Secondary micro- and nanoplastic particles result from fragmentation or degradation of larger plastics, also including tyre wear and synthetic textile fibres (Andrady, 2017; Horton et al., 2017). Degradation of plastics into secondary micro- or nanoplastics can be initiated by UV-radiation or thermal energy causing cracking and subsequent oxidative degradation (Ng et al., 2018). Thereby, with successive and continuous degradation of emitted meso- and microplastics the abundance of nano-sized particles in terrestrial ecosystems can be expected to increase with time.

2.2 Sources and pathways of micro- and nanoplastics to terrestrial environments

Primary and secondary micro- and nanoparticles can enter terrestrial environments through different pathways, with different implications for their fate and thus potential concentrations in soils. Three current main routes have been identified by Bläsing and Amelung (2018): 1) inputs associated with agricultural practices, 2) secondary particle release due to fragmentation of plastic products during their use phase entering soils with runoff or by atmospheric deposition, or 3) fragmentation of individual intentional as well as accidental littered plastics.
In agricultural systems, utilization of soil amendments such as sewage sludge or compost as fertilizer is common practice. Nizzetto et al. (2016) found that within Europe, application rates of sewage sludge to agricultural land ranged between 0-93 %, with an average of 43 %. Although within the EU regulations are in place to restrict the application of sewage sludge if thresholds of risk substances are exceeded, most do not yet include small plastics in their assessment (*86/278/EEC*; Horton et al., 2017; Nizzetto et al., 2016). Conversely, sewage sludge is currently recognized as a major input of plastics from industrial and household use via wastewater streams to terrestrial ecosystems. In municipal wastewater treatment plants, approximately 90 % or more of microplastics and smaller sized particles are efficiently removed from the effluent (Bläsing and Amelung, 2018; Mitrano et al., 2019; Nizzetto et al., 2016). As a result, micro- and nanoplastics are mostly retained in the sewage sludge forming associations with biosolids (Mitrano et al., 2019). Filter steps as well as other pre-treatments have so far proven unsuccessful in removing these particles from sludge or compost (Bläsing and Amelung, 2018; Horton et al., 2017). First estimates for annual maximum loadings for microplastics to soils on an annual EU scale were approximately 63,000 to 430,000 tonnes (Nizzetto et al., 2016). Due to challenges in detection, especially associated with the nano-sized fractions, actual concentrations could be higher than reported and estimates have to

be treated with care. In recent years, member states have been implementing increasingly stricter limitations in national legislation for sewage sludge, partly effectively ceasing its application on agricultural fields (Milieu Ltd et al., 2010; Ministry of Environment, 2018). Despite stricter legislation, agriculture will remain a relevant pathway for input estimations and fate modelling of nanoplastics. This is firstly, due to the long history of sludge application in Europe and secondly, because of continued more direct and intended inputs of plastic related to agricultural land use. These include plastic mulching and packaging materials, polymer coatings for controlled seed germination or encased pesticides, (Horton et al., 2017). Irrigation water is a potential input of concern for areas with no or low pre-treatment of wastewater, especially for areas in close vicinity to urban centres where high microplastic concentrations have been reported (Bläsing and Amelung, 2018; Gewert et al., 2017).
Simultaneously, other more diffuse plastic emissions are likely to gain importance for rural as well as urban soils. That comprises in particular emissions related to wear processes of plastic products during their use phase, including tire abrasion, fragments of paints and fibres from household dust that are mediated by runoff and wind action (Kawecki and Nowack, 2019; Magnusson et al., 2017). Comprehensive quantifications of this second major pathway are still lacking. For tire wear alone LTU (2014) reported that during its lifespan a tire loses approximately 20 % of its total weight to abrasion. Affected by the emissions are road sides, but also especially soils in urban areas with potential implications for human health. Recent investigations by Bergmann et al. (2019) are indicating that microplastics can even be transported over large distances through atmosphere and then be deposited contributing to the exposures of remote terrestrial ecosystems.
Mismanaged waste is the third major contributing pathway. Within the EU, Horton et al. (2017) estimated the mismanaged plastic waste at approximately 520 000 metric tonnes, corresponding to 2 % of total plastic waste, that are released to the environment annually. As plastic production is continuously rising, so are estimates of mismanaged plastic waste released to the environment (Lebreton and Andrady, 2019). Especially in areas where waste management systems are lacking capacities and connection, this pathway may gain relative importance.

2.3 Fate and transport processes affecting particles in saturated porous media

With precipitation, or in agricultural soils irrigation, dispersed particles may be subject to advective transport into lower depths with percolating water through the soil pore systems. As a result of micro-scale transport processes, suspended particles collide with particles of the bulk soil or other colloids present in the soil pore water (Figure 1A). Thereby, fate processes take place that affect their mobility and environmental fate (Figure 1B). Due to a lack of knowledge about nanoplastic transport in soils, fate processes that have been investigated for colloids in saturated soils are used as a first reference. Figure 1B is a simplified overview of these fate processes comprising homo- and heteroaggregation, straining, attachment, detachment and interactions with dissolved organic matter.

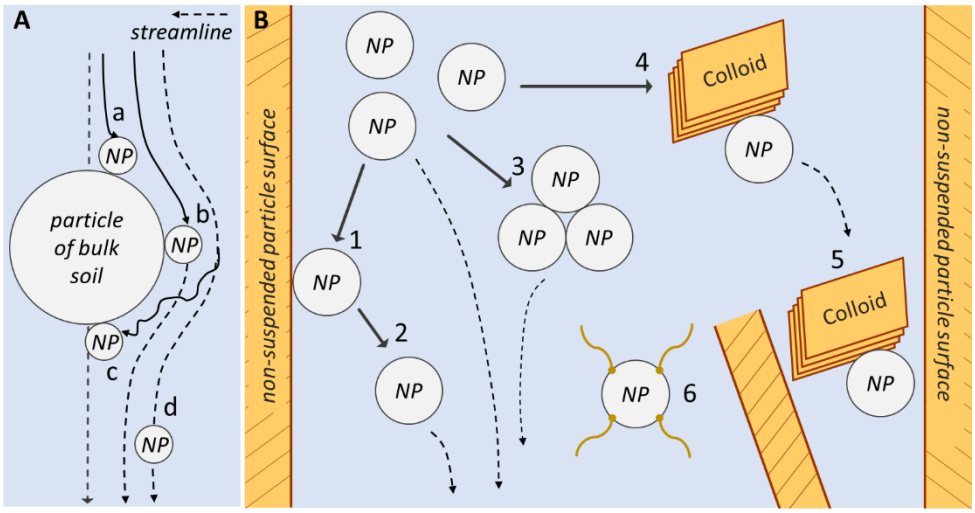

Figure 1: Transport mechanisms and interactions potentially affecting mobility of nanoparticles in saturated soils (simplified overview). A: Physical transport processes modified according to Yao et al. (1971), a) gravitational sedimentation, b) direct interception, c) Brownian diffusion and d) advective transport. B: Mobility affecting interactions modified according to Cornelis et al. (2014), 1) attachment, 2) detachment, 3) homoaggregation, 4) heteroaggregation, 5) straining, and 6) interactions with DOM.

Transport dynamics and interaction forces according to colloid filtration theory

A variety of interactions between suspended particles and soil constituents may affect particle mobility in saturated soils. According to classic colloid filtration theory (CFT) the removal of particles from a suspension in a porous media is a two-step process: 1) establishment of contact through transport, and 2) the association of a particle with a collector surface of the porous media (Yao et al., 1971). Apart from advective transport with water, three physical transport mechanisms are crucial for establishing contact on a micro-scale: Brownian diffusion, direct interception and gravitational sedimentation (Figure 1A). For small particles, diffusion is considered the operative mechanism (Tufenkji and Elimelech, 2005; Yao et al., 1971). With the particle approaching the solid-water interface of another solid, so-called Derjaguin-Landau-Verwey-Overbeek (DLVO) forces may act on the particle. They comprise London–van der Waals attraction and electrical double layer (EDL) repulsion. Van der Waals attraction is related to the separation distance between the surfaces. EDL repulsion occurs when the diffuse double layers of similarly charged particles overlap (Elimelech et al., 1995; Liang et al., 2007). In order for associations to occur under unfavourable conditions, i.e. if suspended particles are similarly charged as the collector surface, this electrostatic barrier has to be overcome (Elimelech et al., 1995; Shen et al., 2010). EDL repulsion is dependent on ionic strength of the medium, as it affects the thickness of the diffuse double layer, and pH as it may affect the surface charge (Cornelis et al., 2014). For removal of particles from the bulk solution, classic CFT only considers one process caused by DLVO forces relevant, i.e. attachment. While some of the fate processes depicted in Figure 1B are a result of DLVO forces, others are affected by so-called non-DLVO forces or physical soil

properties, such as pore size, connectivity and permeability (Bradford et al., 2004). In the following, underlying mechanisms of these fate processes and potential influence on particle mobility are briefly described.

Attachment

The association of suspended particles with reactive immobile particle surfaces of a saturated soil matrix is referred to as attachment (Figure 1B.1). Attachment of particles occurs directly to surfaces of same and opposite charge, or to previously attached particles (Baalousha et al., 2016; Cornelis, 2015; Elimelech et al., 1995). It effectively causes an immobilization of the previously suspended particle and is accordingly regarded as the major determinant of particle mobility in soils. Under favourable conditions, i.e. when particle and collector surface are of opposite charge, attachment occurs more readily (Cornelis et al., 2014). Polystyrene micro- and nanoplastics have been reported to display negative surface charges, either due to material properties, coatings or adsorbed organic molecules (Chinju et al., 2001; Mitrano et al., 2019). Previous research on engineered nanoparticles with negative surface charges identified positively charged clay edges and iron- or aluminium-(hydr)-oxides as preferred sites for attachment (Baalousha et al., 2016; Cornelis et al., 2014). As pH-variable charge sites they display a positive net charge at pH values below a mineral-specific point of zero charge (Supplementary Table S1) (Essington, 2004; R. Xu et al., 2016). In classic CFT, all collisions of particles with the bulk soil result in irreversible attachment (Elimelech et al., 1995; Yao et al., 1971). More recent approaches acknowledge that detachment of particles is possible and try to incorporate it into conceptual models (Shen et al., 2012; S. Xu et al., 2016).

Detachment

The physical and chemical processes involved in detachment of particles from the bulk soil are substantially different from attachment. In order for a particle to be detached external forces must be applied that exceed the forces holding the particle attached (Cornelis, 2015; Praetorius et al., 2014). It is more likely for particles held in weak associations, and under unfavourable conditions hydrodynamic forces may suffice to cause detachment (Kuznar and Elimelech, 2007). Detached particles continue moving through the porous media primarily, making them subject to attachment or straining (Bradford et al., 2007).

Homo- and heteroaggregation

Processes affecting mobility of particles can similarly occur with other particles suspended in the soil pore water. Aggregation describes the association of mobile particles in clusters as permanent contacts are established upon collision. For particles of the same material the term homoaggregation is used (Figure 1B.3). Heteroaggregation occurs between unlike particles and more readily for particles of opposite surface charge (Figure 1B.4) (Baalousha et al., 2016; Elimelech et al., 1995). As Brownian motion is inversely related to particle size, any form of aggregation theoretically results in reduced mobility. Conversely, a reduced surface charge due to aggregation may allow further transport as attractive DLVO-forces are reduced (Cornelis et al., 2014). Previous studies by Mitrano et al. (2019) show that heteroaggregation is relevant for nanoplastics, as 98 % aggregated with particles of

sewage sludge in batch tests. With respect to higher abundancy of non-plastic colloids in soils, heteroaggregation is more likely to be relevant for non-point sources.

Straining and size exclusion

Straining refers to the retention of colloidal particles based on physical filtering when interstices between adjacent particles of the soil matrix are too small for passage (Figure 1B.5) (Bradford et al., 2004; Xu et al., 2006). It occurs irrespective of the chemical composition of the solution or electrostatic interactions and is primarily influenced by physical parameters such as average grain diameter ratio, soil particle shape and roughness (Bradford et al., 2004; Tufenkji et al., 2004). Hetero- and homoaggregation contribute to higher susceptibility of particles to straining as a direct consequence of increase in size with aggregate formation (Baalousha et al., 2016). In addition to straining, aggregation can amplify size exclusion due to preferential flow of larger suspended particles in larger pores, also referred to as colloidal pumping (Bradford et al., 2004; Cornelis et al., 2014).

Interactions with dissolved organic matter and steric stabilization

Natural soils contain organic matter, part of which is present as dissolved organic matter (DOM) defined by sizes below 0.45 µm (Zsolnay, 2003). Adsorption of DOM to the suspended phase may be driven by opposite charges, or due to relative hydrophobicity of both materials which occurs irrespective of charge (Elimelech et al., 1995; Praetorius et al., 2014). Steric and electrostatic stabilization may enhance particle mobility. Electrostatic stabilization occurs if the adsorbed molecule increases the surface charge of the particle (Phenrat et al., 2008). Steric stabilization results from the formation of an adsorbed layer of non-ionic polymers which functions as a physical barrier to other surfaces. Often strongly hydrated, this layer produces strong repulsion when compressed upon approach of another surface (He et al., 2019; Phenrat et al., 2008). Plastics are polar and non-polar carbon-based materials, so interactions with DOM in natural soils are likely. Hydrophobic and steric forces acting on particles in the presence of DOM are referred to as non-DLVO forces (Figure 1B.6).

Degradation

Most plastics are highly insoluble and highly resistant to degradation with very long half-lives (Andrady, 2017; Auta et al., 2017). Thus, for short-term exposure levels, degradation is often neglected as a pathway. However, for long-term assessments degradation may be crucial to consider since particle sizes decrease with time, possibly changing the fate of plastics in soils.

Interactions in unsaturated porous media

In unsaturated soils, a range of additional processes may affect particle transport. In general, the presence of air in the soil pore system is associated with higher retention of particles as they may attach to air-water and air-water-solid interfaces, or be retained by strong capillary forces at the air-water-solid interface (Lazouskaya and Jin, 2008; Torkzaban et al., 2008; Xu et al., 2006). In addition, as soil pores become successively air-filled, higher proportions of stagnant water are encountered

characterized as low flow velocity regions promoting the occurrence of straining (Fujita and Kobayashi, 2016; Torkzaban et al., 2008).

2.4 Advection-reaction-dispersion equation for solute and particle transport in porous media

Quantitative fate descriptors are used in risk assessments to predict the behaviour of harmful dissolved substances in soils. Recently, their suitability for describing the movement of particulate substance is being tested. For describing one-dimensional transport of solutes, numerical solutions to the advection-reaction-dispersion (ARD) equation have been developed. The ARD equation comprises terms for the major transport mechanisms of solutes and particles, as well as for chemical interactions that occur in contact with soil constituents (Šimůnek et al., 2009). Advection is the transport of the substance in bulk motion, while hydrodynamic dispersion summarizes the movement due to concentration gradients, including microscopic diffusion and macroscopic mechanical dispersion. In combination, the separate processes of the ARD equation are used to determine the concentration of a substance with respect to time and distance under consideration of Fick's law for diffusion and the conservation of mass law for the different transport mechanisms (Šimůnek et al., 2009, 2008):

$$\frac{\partial C}{\partial t} = -v\frac{\partial C}{\partial x} + D_L\frac{\partial^2 C}{\partial x^2} - \frac{\partial q}{\partial t} \qquad \text{(Equation 1)}$$

with C as the concentration in the aqueous phase (M V^{-3}), t as time (T), v is the pore water flow velocity (L T^{-1}), x refers to distance (L), D_L the hydrodynamic dispersion coefficient (L^2 T^{-1}) and q the substance concentration associated with the solid phase (M M^{-1}) (Bradford et al., 2004; Šimůnek et al., 2009). Note that M represents mass units, V volume units, T time units and L length units in this context. The first, second and third term on the right represent advection, dispersion and chemical interactions (Bradford et al., 2003; Šimůnek et al., 2009). The chemical interaction term describes the change of concentration in the aqueous phase as a result of equilibrium and non-equilibrium interactions with the solid phase (Šimůnek et al., 2009). Underlying assumptions in Equation 1 are a stationary water flow and a homogenous porous medium. In order to describe the transport of colloidal particles in kinetic terms, the ARD equation (Equation 1) is modified for colloid transport to include kinetically described mass transfer from the aqueous phase to different sites of the solid phase and vice versa. The colloid mass balance equation thereby becomes Equation 2:

$$\frac{\partial \theta C}{\partial t} + \rho_b\frac{\partial S_1}{\partial t} = \frac{\partial}{\partial x}\left(\theta\, D_L\frac{\partial C}{\partial x}\right) - \frac{\partial q}{\partial t} \qquad \text{(Equation 2)}$$

where θ is the volumetric water content (V^3 V^{-3}), ρ_b is the dry bulk density (M V^{-3}), C refers to the number concentration in the aqueous phase (N_c V^{-3}) and S_1 to the number concentration in the solid phase (N_c V^{-3}). The solid phase S_1 represent kinetic sorption sites (Bradford et al., 2004; Šimůnek et al., 2009). Although it is possible to include terms for degradation, the long-term fate of plastics is insufficiently investigated, thus neglected in this study. First-order kinetic processes are described

by Equation 3. It accounts for interactions between dispersed particles and the bulk soil considered most relevant for mobility, i.e. attachment and detachment:

$$\rho_b \frac{\partial S_1}{\partial t} = \theta\, k_{att}\, C - \rho_b\, k_{det}\, S_1 \qquad \text{(Equation 3)}$$

where k_{att} is the first-order attachment coefficient (T^{-1}), and k_{det} the first-order detachment coefficient (T^{-1}). Both coefficients are reported strongly affected by water content of the soil, with increasing attachment as water content decreases (Šimůnek et al., 2009). If all parameters are known, the equation can be numerically solved and the fate of particles in soils simulated to predict their mobility and potential risk for accumulation or leaching.

Attachment efficiency

The collision or attachment efficiency of nanoparticles is increasingly reported as the material-specific parameter describing transport in soils (Cornelis et al., 2013; Raychoudhury et al., 2010). In principle, it can be used to predict retention of particles in soils by calculating the attachment rate constant k_{att} which can be determined by Equation 4 as a function of the attachment efficiency α_{att}:

$$k_{att} = \alpha_{att} \frac{3\,(1-\theta)}{2 d_{50}} \eta_0 v \qquad \text{(Equation 4)}$$

with the single-collector removal efficiency η_0 (-), and d_{50} as the median of the grain diameter (L) (Bradford et al., 2004; Šimůnek et al., 2009). The attachment efficiency α_{att} describes the fraction of particle collisions with collector surfaces that result in attachment (Solovitch et al., 2010). It is often empirically determined using experimental breakthrough curves (BTC) in standardized column leaching tests (Bradford et al., 2007; Cornelis, 2015; OECD, 2004). It is thus also an empirical factor, though it could also be calculated in theory from the net effect of attractive and repulsive DLVO and non-DLVO forces (Bradford et al., 2004). The single-collector contact efficiency is proportional to the collision frequency and accounts for the effect of immobilization of particles through diffusion, direct interception and gravitational sedimentation. The attachment rate constant (k_{att}) is highly dependent on hydrodynamic conditions and thus remains tied to the specific conditions under which it has been determined.

2.5 Particle mobility affected by bioturbation

While the previous chapter focused on advective transport and interactions between suspended dispersed particles and soil constituents, the following is aimed at drawing attention towards the role of living organisms for the mobility and spatial redistribution of particles in soils. Bioturbation describes the physical displacement of solutes and solids in soils caused by the activities of organisms (Wilkinson et al., 2009). Groups of soil organisms that are in particular associated with biogenic translocation of soil constituents are earthworms (*Lumbricida*), ants (*Formicidae*) and termites (*Isoptera*) (Blume et al., 2016). In the context of particle pollution and risk assessment, earthworms are of specific interest due to their burrowing activity and thus role in vertical displacement of particles throughout the soil profile. A recent

study by Baccaro et al. (2019) has demonstrated that engineered nanoparticles which tend to accumulate in upper layers of soils were more significantly displaced through bioturbation than via advection. Thus, it is crucial to include biologically mediated transport into mobility and exposure assessments of particles in soils. This applies to particles of otherwise low mobility through advective transport (Baccaro et al., 2019; Jarvis et al., 2010), but also to more mobile particles as distribution into lower soil layers may be substantially enhanced through earthworm activity.

Bioturbation by earthworms and its impact on particle mobility

The biologically mediated transport caused by earthworms comprises different processes that are initiated by their burrowing activity: 1) mechanical mixing, 2) spatial separation of ingestion and excretion or adhesion and release, and 3) improvement of soil structure and macropores enhancing preferential flow. Burrowing activity directly causes a displacement of soils through mechanical mixing (Wilkinson et al., 2009). First results from a bioturbation study by Huerta Lwanga et al. (2017) found that high amounts of microplastics from surface litter were incorporated into burrow walls of earthworms. Bioturbation through ingestion and adhesion to the organism surface may be of considerable importance for nanoplastics, as they are potentially more susceptible to uptake due to their smaller size (da Costa et al., 2016). Frequently referred to as environmental engineers, earthworms also modify soil physical properties through formation of burrows and increasing aggregate formation by egestion as well as mixing organic matter into lower depth (Meysman et al., 2006). Resulting macropores are routes for preferential flow of percolating water, increasing leaching of especially particulate or colloid-bound nutrients and pollutants (Bardgett, 2005). Thus, changed soil porosity by earthworms may facilitate the transport of small plastics not only from surficial soil layers, but also of plastics previously deposited into the burrow walls with earthworm movement (Huerta Lwanga et al., 2017).

However, adaptive strategies vary among earthworm species, resulting in different temporal and spatial foraging and burrowing patterns that affect their bioturbation efficiency (Taylor et al., 2018), and thereby particle mobility. In general, earthworms are distinguished into three ecological types: epigeic, endogeic and anecic (Bouché, 1977). While epigeic species primarily remain within the humus layer of soils, endogeic and anecic species are burrowing earthworms and therefore considered more relevant for studies on vertical transport of particulate pollutants, such as nanoplastics. Endogeic species, such as *Lumbricus rubellus*, are shallow-burrowing and consume soil along with their food. Opposed to that, anecic earthworms, such as *Lumbricus terrestris*, feed on litter on the surface and then create deep vertical burrows for refuge (Blume et al., 2016; Fründ et al., 2010; Huerta Lwanga et al., 2017). Bioturbation intensity further depends on whether soil chemical and physical conditions are favourable for the particular earthworm species. This includes air and water content, food and nutrient availability, temperature as well as soil texture, with specific requirements differing between species (Blume et al., 2016; Taylor et al., 2018).

2.6 Quantification of transport by bioturbation

For quantitatively describing and predicting the transport of pollutants by bioturbation, models based on mixing efficiencies or mixing rates can be used. While mixing efficiencies are easily obtained from empirical data, mixing rates are semi-empirical models that aim to mathematically describe the effect of bioturbation as a function of time under consideration of different processes. The bioturbation model developed by Rodriguez (2006) provides a tool for predicting the spatial distribution of particles in a soil modified by the mixing effect of earthworm activity. The model has been successfully implemented to predict nanoparticle concentrations in the bioturbation study by Baccaro et al. (2019). It is a one-dimensional mathematical model based on a bioturbation rate through which depth-dependent substance concentrations in a soil can be predicted as a function of time. The model is based on parameter fitting to observed experimental data to determine the bioturbation rate. For this purpose, the given soil column is segmented into separate layers (n=L) of a specific depth d_l (m). Each layer is associated with a concentration C (mg kg^{-1}) that is assumed constant within the layer and estimated for different times at defined timesteps δ_t (s) (Baccaro et al., 2019; Rodriguez, 2006). The bioturbation rate k_{bioturb} (s^{-1}) is calculated according to Equation 7 from the soil turnover rate $v_{:l+1}$ (m s^{-1}) and the specific depth step d_l, with each layers concentration then determined by Equation 8:

$$k_{bioturb,l:l+1} = \frac{v_{l:l+1}}{d_l} \qquad \text{(Equation 7)}$$

$$[C]_{l,t+x} = [C]_{l,t} + k_{bioturb,l:l+1,t}\,\delta t\left([C]_{l+1,t} - [C]_{l,t}\right) + k_{bioturb,l-1:l,t}\,\delta t([C]_{l-1,t} - [C]_{l,t}) \qquad \text{(Equation 8)}$$

Mixing during each defined timestep is restricted to the directly adjacent layers below *l+1* and above each layer *l-1*. It is assumed to be instantaneous and directly proportional to earthworm density w_l (individuals m^{-3}) and is determined by implementing a bioturbation fitting parameter β (m^4 s^{-1}) (Rodriguez, 2006):

$$v_{l:l+1} = \beta w_l \qquad \text{(Equation 9)}$$

where the bioturbation fitting parameter needs to be fitted by implementing Equation 8 to compare modelled with experimental data (Baccaro et al., 2019). With the fitted bioturbation rate, predictions can then be made on the spatial distribution of particles and the time it takes for a specific soil with a specific worm density to be completely mixed. Complete mixing is described by Baccaro et al. (2019) as the timepoint at which differences in concentrations between adjacent layers is within a range of 10 µg kg^{-1}. Determining the time span it takes for complete mixing can then be used to assess the incorporation of nanoplastics into deeper soil layers after application to soils.

3 Materials and Methods

3.1 Soil characterisation

For column leaching tests and bioturbation plots, a soil from a formerly agricultural site in Sprowstown, Norfolk, United Kingdom, was used. A summary of relevant soil characteristics is provided in Table 1. The topsoil was classified as sandy loam with a relatively high pH, likely related to former agricultural use. Approximately half of the organic matter is generally assumed to be organic carbon (Blume et al., 2016; Chapin et al., 2002). Corresponding organic carbon contents of 2.5 % w/w were representative for plough horizons (Wiesmeier et al., 2012). The soil contained anthropogenic inorganic components, i.e. brick fragments. As plastics were doped with palladium (Pd), the background concentration in the soil was separately measured by applying *aqua regia* extractions (section 3.3.2). The resulting Pd-background concentration was 32 ± 4 µg kg^{-1}. Previous studies found strongly enhanced Pd-concentrations in soils near roadsides or within urban centres, related to abrasion from vehicle exhausts (Cicchella et al., 2003; Wichmann et al., 2008). With regards to the reported maximum values in these studies (43-124 µg kg^{-1}) and the close vicinity of the sampling site to roads and the city centres of Sprowston and Norwich, the detected concentrations were considered representative for this area.

Table 1: Selection of physical and chemical soil properties. Data denoted with a was provided by Bailey's of Norfolk Ltd., b was based on own measurements.

Selected soil characteristics						
pH[a,b]		7.2-7.6	Soil texture [a]			
carbonates[a]	*% w/w*	1.0	coarse fragments	2-20 mm	*% w/w*	3.4
organic matter[a]	*% w/w*	5.0	sand	2.0-0.06 mm	*% w/w*	60.0
available P[a]	*mg L^{-1}*	49	silt	0.06-0.002 mm	*% w/w*	28.0
Pd[b]	*µg kg^{-1}*	32 ± 4	clay	<0.002 mm	*% w/w*	12.0
WHC[a]	*mL kg*	420				

3.2 Characterisation of nanoplastics

The synthesized plastic particles consisted of a polyacrylonitrile (PAN) core in which the palladium used for tracing was embedded, surrounded by a crosslinked polystyrene (PS) shell (Mitrano et al., 2019). Their raspberry-like surface morphology is shown in Figure 2A. While the core material provides the primary matrix for the metal tracer, the PS shell material determines the interactions the particles are engaging in. PS is more widely used and thus, more relevant for environmental risk assessments than PAN (Mitrano et al., 2019; Ng et al., 2018). PS is a synthetic aromatic hydrocarbon polymer that consists of multiple interconnected styrene monomers $(C_8H_8)_n$, as displayed in Figure 2B. It consists of a very resistant linear polyethylene chain connected over carbon-carbon bonds, with phenyl rings attached laterally. General-purpose polystyrene has a density of 1.05 g cm^{-3} (Scheirs and Priddy, 2003). Although secondary plastics predominate in the environment (Andrady, 2017), using synthesized primary nanoplastics provides the advantage of reduced heterogeneity and facilitates parameterization and modelling processes. The nanoplastics did not contain any further additives. However, sodium dodecyl sulfate was used as a surfactant to keep the suspensions stable during synthesis. The metal content of the nanoplastics was considered a suitable proxy for particle concentrations by Mitrano et al. (2019) who measured the Pd-concentrations of nanoplastic suspensions in serial dilutions, confirming a linear decline. The synthesized nanoplastic particles utilized in this study were from newly generated batches supplied by the Swiss Federal Aquatic Research Institute (Eawag). As displayed in the overview (Figure 3), the nanoplastic suspensions were characterized in more detail with regards to their particle mass concentration, their particle size and zeta potential and the corresponding palladium content obtained by different pre-detection preparation steps.

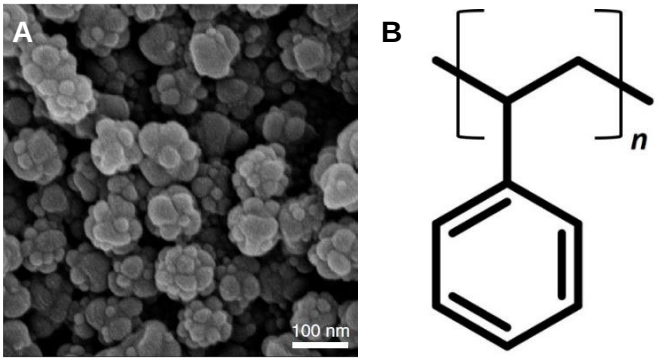

Figure 2: Synthesized nanoplastics used for transport studies: A) Image of raspberry-shell nanoplastics by Mitrano et al. (2019). Note that the image displays particles of a previous batch produced so sizes differ for the particles used in this study; B) Chemical structural formula of the shell material polystyrene modified according to Scheirs and Priddy (2003).

3.2.1 Particle and palladium concentrations

Three replicates of 0.5 mL stock solution were oven-dried at 60°C for 48 hours to determine mass concentrations of plastics in the provided stock solution. The measured particle weight corresponded to 117 ± 0 g L^{-1}. Palladium concentrations were obtained by acid extraction and direct injection (section 3.3, Figure 3). The most efficient method for palladium recovery resulted in a Pd-concentration in the stock solution corresponding to 281 ± 4 mg L^{-1}. Accordingly, the Pd-content corresponded to 0.24 % m/m of the particle weight for the used nanoplastics.

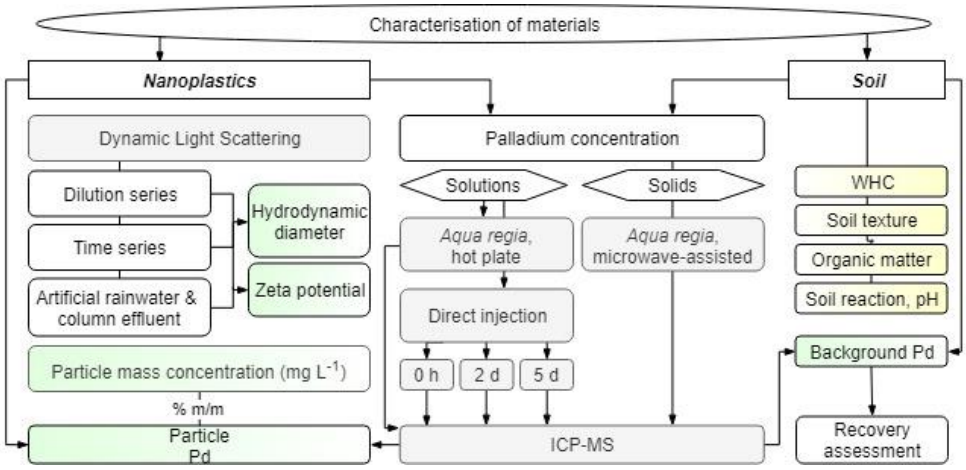

Figure 3: Overview of the materials used in the study and analytical steps taken for soil and nanoplastic characterisation. Marked are analytical methods (grey), measured parameters (green) and externally analysed parameters (yellow).

3.2.2 Nanoplastic particle size and zeta potential based on Dynamic Light Scattering measurements

Dynamic light scattering for determining particle size

Dynamic Light Scattering (DLS) on a Malvern Zetasizer Nano ZS instrument was used for determining hydrodynamic particle diameter and estimating surface charge. Size measurements by DLS are based on detecting the intensity of incident light from a laser that is scattered by dispersed particles which are moving due to Brownian motion. As velocity of movement is inversely related to particle size, the instrument converts a derived translational diffusion coefficient to the hydrodynamic radius of a solid spherical particle (Bhattacharjee, 2016; Ramos, 2017). The hydrodynamic diameter includes molecules and solvents that form coating layers and move at the same speed as the assayed dispersed phase. It is therefore larger than the actual solid particle radius (Bhattacharjee, 2016).

For this study, backscatter detection (scattering angle 173°) was performed on 1-1.5 mL samples of particles diluted with ultrapure water in disposable optical polystyrene macrocuvettes (VWR). Prior to use, the cuvettes were successively rinsed

with ethanol and ultrapure water. Experimental conditions and quality criteria for measurements are listed in the Supplementary Table S2. The hydrodynamic, or Z-average, diameter was calculated based by cumulative method, chosen due to its lower insensitivity to noise (Bhattacharjee, 2016).
Measurements were conducted on samples over a dilution series to minimize multi-scattering and account for effects of interparticle interactions (Bhattacharjee, 2016; Ramos, 2017). The mean particle size obtained from the dilution series was 256 ± 4 nm diameter. The size increase over dilution steps was linear, although non-significant ($p>0.05$). The polydispersity index (PDI) describes the relative homogeneity of particle sizes (Bhattacharjee, 2016; Ramos, 2017). With a mean PDI of 0.096, the dispersion was considered highly monodisperse. The particle suspensions were re-measured in a time series over a period of five weeks applying the same particle concentration (170 mg L^{-1}). The observed trend of decreasing diameter size with time, i.e. from 255 ± 2 nm to 251 ± 5 nm, was non-significant ($p>0.05$). The diluted suspensions were therefore considered stable for at least 5 weeks. Measurement conditions and results are listed in Supplementary Table S3 and S4.

Dynamic light scattering for determining Zeta potential

Zeta potential measurements by the Malvern Zetasizer Nano ZS are based on the electrophoretic mobility of particles, for which a high frequency electric field is applied on the suspension that causes charged particles to move towards the opposite electrode. Particle velocity is measured through light scattering using Laser Doppler Velocimetry, and then converted to Zeta potential (Malvern Instruments Ltd., 2009). The obtained Zeta potential refers to the surface potential at the slipping plane of the particles. This plane represents the interface between the medium and the particle with bound ions that are moving at the same speed as the electrical field is applied. The slipping plane includes the Stern and parts of the diffuse layer of the electric double layer, and thereby does not represent actual particle surface charge density (Bhattacharjee, 2016). Zeta potential is used to assess the stability of colloids, and is generally considered stable at values higher than +30 mV or lower than -30 mV (Malvern Instruments Ltd., 2009).
For the Zeta potential measurement, samples of approximately 1-1.5 mL volume were injected into a folded capillary cell with a syringe. The measured Zeta potential was -60 ± 1 mV in ultrapure water, and nanoplastics therefore found stable. The relatively high potential is likely caused by the anionic surfactant used as dispersant during production of the particles.

Repeated characterization in artificial rainwater and effluent

The hydrodynamic radius as well as Zeta potential are affected by conditions modifying the electric double layer and its thickness, including ionic strength or pH of the surrounding dispersion medium. Therefore, measurements were repeated using artificial rainwater that was used as dilution medium in following column tests, and in centrifuge filtered effluent from saturated columns (10 K). Although non-significant ($p>0.05$), the measured hydrodynamic radius in ultrapure water was larger than in other media as in accordance with theory (Bhattacharjee, 2016; Ramos, 2017). The Zeta potential remained stable in artificial rainwater but was significantly different in the effluent ($p<0.05$)(Table 2). Zeta potential is affected by solvents present

in the solution (Bhattacharjee, 2016). Thus, it is possible that the surfactant interacts with dissolved substances in the effluent. Nevertheless, the dispersion was considered stable (below -30 mV).

Table 2. Overview of Zeta potential and size measurements of nanoplastics in different dilution media, including ultrapure water, artificial rainwater and effluent from soil columns.

Comparison of dilution medium	Zeta potential (mV)	Z-average diameter (nm)
Ultrapure water	-59.5 ± 1.0	256 ± 4
Artificial rainwater	-57.3 ± 1.5	247 ± 3
Effluent	-38.1 ± 1.1	246 ± 6

3.3 Analytical methods for palladium detection

Inductively coupled plasma mass spectrometry (ICP-MS) was used for detection of palladium in liquid samples. After establishing the Pd-concentration of the nanoplastics and the background concentrations in the soil, it was used to quantify nanoplastics in soil and effluent samples from advective transport studies, as well as from bioturbation tests. The speciation and solubility of palladium was predicted using simulations in Visual MINTEQ. Different methods for sample preparation were applied to determine the method of highest recovery, including repeated direct injection of diluted particle suspensions in the ICP-MS over a time series, acid digestion in open-vessel and in closed-vessel systems (Figure 3).

3.3.1 Simulation of behaviour of dissolved palladium in Visual MINTEQ

Dissolved palladium $[Pd^{2+}]_{(aq)}$ readily forms dissolved hydroxide and hydroxy-chloride complexes, but can also precipitate as amorphous $Pd[OH]_{2(s)}$ under specific conditions. Its solubility depends to a large extent on the pH of the solution and its composition, investigated in detail by van Middlesworth and Wood (1999). Generally, with increasing pH the proportion of palladium-hydroxides increases, and precipitation of $Pd[OH]_{2(s)}$ can occur if solutions are oversaturated. In chloride containing samples the solubility is primarily controlled by the following reaction (van Middlesworth and Wood, 1999):

$$Pd[OH]_{2(s)} + 2H^+ + nCl^- \rightleftarrows PdCl_n^{2-n} + 2H_2O_{(l)} \qquad \text{(Equation 10)}$$

with values between 0-4 for *n*, indicating a strong dependence on the chloride concentration of the solution (van Middlesworth and Wood, 1999). The resulting dissolved palladium(II)-chloride species that would be expected in solution are: $[PdCl_4]^{2-}_{(aq)}$, $[PdCl_3]^{-}_{(aq)}$, $[PdCl_2]_{(aq)}$ and $[PdCl]^{+}_{(aq)}$. Thereof, tetrachloropalladate(II) $[PdCl_4]^{2-}$ is the most stable dissolved complex (van Middlesworth and Wood, 1999). In order to assess the stability of solutions containing dissolved Pd-species measured on the ICP-MS, the freeware Visual MINTEQ 3.1 was used for simulating speciation and saturation indices under different additions of hydrochloric acid (Gustafson, 2013). The expected dominant species could thereby be estimated. Using expected post-extraction concentrations of 2.78 % HCl, the solution remains undersaturated. Palladium is expected to remain totally dissolved as $[PdCl_4]^{2-}_{(aq)}$, and to a

lesser extent as $[PdCl_3]^-_{(aq)}$ and $[PdCl_2]_{(aq)}$ (Supplementary Table S5). Including solid phases as competing sorption places in the simulation increased the saturation index slightly which may be relevant if residues of soil are present. The dominant complex expected in ultrapure water would be $[PdOH]^+$. Note, that in the absence of Cl-ions, the solution would be oversaturated and precipitation of Pd as $Pd(OH)_{2(s)}$ would be possible (Supplementary Table S5). Maintaining the chloride concentration at high enough levels to prevent oversaturation was therefore crucial for the sample preparation in this study.

3.3.2 Sample preparation methods: direct injection and acid extraction

Direct injection of suspensions containing nanoplastics

Suspensions containing nanoplastics that were directly injected into the ICP-MS were diluted with ultrapure water or artificial rainwater from stock solutions, either according to targeted dilution factors or as leachates of unknown concentrations. Generally, injection was performed as soon as possible after sample preparation without further treatment steps.

Acid extraction with aqua regia in hot plate and microwave-assisted systems

Acid extraction was used for the characterization of nanoplastics to determine Pd-concentrations in aqueous solutions and to determine the Pd-recovery from soil samples containing these nanoplastics. Acid digestions of diluted nanoplastic suspensions were conducted in two different setups, 1) *aqua regia* in an open-vessel hot plate arrangement, and 2) *aqua regia* in a pressurized closed-vessel microwave-assisted system. *Aqua regia* is a solvent mixture of highly concentrated nitric acid (65 vol.%, suprapure HNO_3) and hydrochloric acid (37 vol.%, suprapure HCl), typically in a volumetric ratio of 1:3. It is a standardized extraction method commonly used for trace element analysis in environmental samples (ISO 11466:1995). In the following, the protocols applied in this study are briefly summarized. Microwave-assisted extraction is usually preferred as in closed vessels under pressure samples can be heated above their boiling temperature, and at higher power, generally increasing the recovery efficiency (Destandau et al., 2013). Open-vessel digestion results in less acid and less diluted extracts, suitable for samples of very low concentrations more realistic in environmental samples. Conversely, it is less efficient, and sample might be lost during heating.
Prior to digestion, all labware was cleaned and rinsed with ultrapure water before placing it in a 1 vol.% HNO_3 acid bath for at least 12 hours, followed by rinsing and drying. For assessment of the quality of the extractions, every batch included three replicates of each sample, procedural blanks for correction, and spiked samples as recommended by Silva et al. (2018). Spikes were prepared from a 999 ± 2 mg L^{-1} palladium stock solution diluted with 3 vol.% HCl.

Open-vessel hot plate extraction

For the open-vessel extraction, samples were pipetted into 25 mL Teflon (PTFE) tubes and acids added successively to each sample, with 1 mL HNO_3 pipetted

directly onto the sample and 3 mL HCl by rinsing the sides of the tubes. The open vessels were placed on a hot plate. The temperature was kept at 75°C to avoid boiling and sample loss. Samples were heated for 1.5 hours, then allowed to cool down for 30 minutes. Afterwards, they were transferred by repeated rinsing and diluted with 3 vol.% HCl to a final volume of 10 mL. The open-vessel digestion was only performed on aqueous suspensions containing nanoplastics.

Microwave-assisted extraction

A Milestone Ethos Easy microwave equipped with a high-throughput rotor (MAXI-44) was used for the closed pressurized extraction. Due to a minimum volume required, the *aqua regia* consisted of 1.25 mL of HNO_3 and 3.75 mL of HCl. To extract palladium from aqueous suspensions and soil samples, 100 mL lined PTFE vessels with a plug and cap mechanism were used. A sample weight of approximately 0.5 g was required for solids. Weighting floats were used to determine the exact amount of soil added to each tube. Replicates of soil were routinely spiked with solutions of known Pd-concentrations to ensure analytical quality. Samples were added to the extraction vessels first, then one by one treated with the acids: HNO_3 was applied directly onto the sample and HCl rinsed down the sides of the PTFE vessel. The liners were tightly sealed with plug and cap. The microwave programme was set up following EPA 3051a guidelines (U.S. EPA, 2007) and according to producer recommendations. With 1800 W for more than 15 vessels at a time, samples were heated up to 175°C for 20 minutes and kept stable at 175°C for 10 minutes. During the programme, the carousel continuously rotated. After a cooling period of approximately 60 minutes, or until the temperature was below 30°C, the vessel contents were transferred into 50 mL volumetric flasks using a funnel. For samples containing solids this was done by filtering to exclude non-decomposed residues (Munktell filter paper, OOM). To ensure a complete transfer of dissolved palladium, droplets were washed off the plug and the vessels rinsed at least three times and emptied after each rinse. Then, filters and funnels were rinsed, before diluting the sample to a final volume of 50 mL. Ultrapure water was used for rinsing and as post-extraction dilution medium in order to reduce corrosion risk of the instruments, while maintaining a sufficiently high chloride concentration to prevent precipitation of Pd-hydroxides (section 3.3.1).

3.3.3 Palladium detection in solutions via ICP-MS

Inductively Coupled Plasma – Mass Spectrometry (ICP-MS) is a combined detection of elements using an ICP with a mass spectrometer. In short, a liquid sample is converted into a fine aerosol by a nebulizer. The nebulizer gas then carries a small fraction of the aerosol through the spray chamber and injected into a plasma, where the aerosol is vaporized, atomized and finally ionized (Beauchemin, 2017). With electrons being separated from the analyte, a positive ion beam is created that is transmitted to the mass spectrometer. Based to their mass-to-charge ratio ions of target elements are then separated and measured by a detector (Beauchemin, 2017). Detected ion signals are automatically blank corrected and related to external calibrations for conversions to concentrations by the ICP-MS operating software

(Syngistix 2.3). Here, a Perkin Elmer ICP-MS instrument (Nexion 350D) with a quadrupole mass spectrometer and Argon as nebulizer gas was used for detection of palladium in liquid samples. Calibration was done prior to measurements of samples by external standards, prepared from the 999 ± 2 mg L^{-1} palladium stock solution. Supplemented by a blank, the instrument provided calibration curves for each measurement. An internal standard with 5 µg L^{-1} indium was used to correct Pd signals for variations due to instrument drift or ion suppression by other elements present in the sample described in the literature (Beauchemin, 2017; Brenner, 2017). This correction was automatically done by the ICP-MS operating software through converting raw intensities into net intensities by accounting for internal standard signals and blank measurements. For each sample three replicate measurements were conducted with five readings each. After approximately 15-20 samples a blank measurement was conducted. As a dilution medium for standards, internal standard and rinsing solution, 3 vol.% HCl was chosen. This was motivated by two objectives: 1) matrix matching as concentrations of hydrochloric acid of post-extraction samples measured on the ICP-MS were estimated at 2.78 % and 2) assuring no precipitation of palladium would negatively affect the detection. The obtained Pd-concentrations were corrected using concentrations of procedural blanks and backgrounds in case of soil extractions.

3.3.4 Evaluation of analytical methods for Pd-recovery from particles

The above described methods were applied in order to firstly, characterize the nanoplastic stock suspension with regards to its Pd-contents and secondly, to determine the recovery and thereby most suitable method for detection of nanoplastics in suspensions and soils. For this purpose, nanoplastic suspensions of same dilution factor were used for all methods, and either treated with acids, directly injected or applied to soil samples as a spike. For the open-vessel and microwave-assisted *aqua regia* extraction the same solvent-to-feed ratio (4:1) was applied to allow for direct comparison. Direct injection of diluted suspensions into the ICP-MS was performed in a time series: immediately after sample preparation, after two and after five days (Figure 4). Soil was spiked with 1.25 mL of the same dilution for determining the recovery of palladium from nanoplastics in soil samples in the microwave-assisted *aqua regia* setup.

The most efficient method for extracting palladium incorporated into nanoplastics in suspensions was the microwave-assisted digestion (Figure 4). According Pd-concentrations in the stock solution of nanoplastics was thereby estimated at 281.0 ± 3.5 mg L^{-1}. Direct injection of suspensions without further treatment still recovered 90-95 % of this nanoplastic-incorporated Pd-content within the first two days after sample preparation (Figure 4B). The poor performance of the hot plate extraction in Pd-recovery of particles might be related to sample loss during the heating. As direct injection still resulted in good recoveries of palladium it was selected for analyses of suspensions in order to minimize dilution and potential challenges with detection limits of the ICP-MS. Recovery of palladium from nanoplastics in the presence of soil was 91 % after correction for procedural blanks and accounting for the Pd-background concentration of the soil (Figure 4C).

Consequently, the microwave-based aqua regia extraction was suitable for analysing soil samples containing nanoplastics.

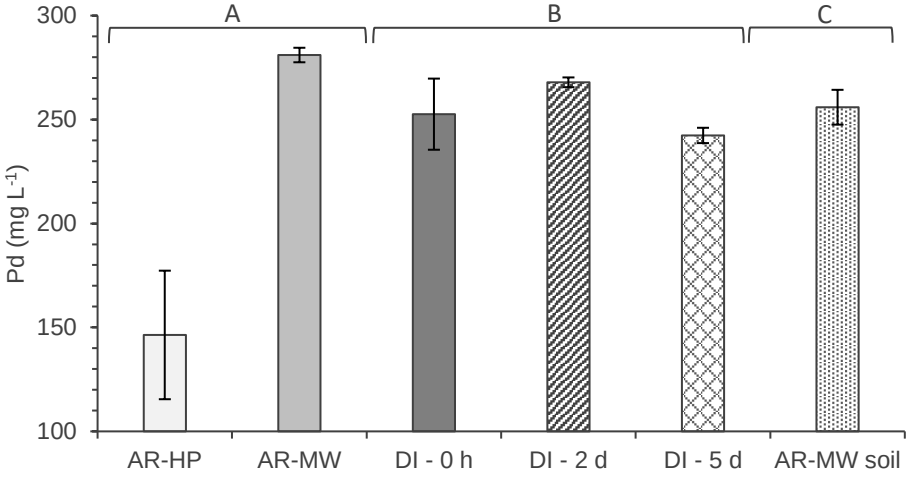

Figure 4: Measured palladium contents of doped nanoplastics via ICP-MS using different preparation methods. A) aqua regia (AR) of suspensions using hot plate (HP) and microwave-assisted extraction (MW), B) direct injection (DI) of suspensions after 0 hours, 2 days and 5 days, and C) microwave-based aqua regia extractions for recovering Pd-recovery of nanoplastics in the presence of soil (corrected for the Pd-background of the soil).

3.4 Column transport studies

Column leaching tests are used in risk assessments to simulate the leaching behaviour of a substance in soils. For this purpose, a column of inert material is packed with disturbed soil to which the test substance and artificial rain is then applied (OECD, 2004). By collecting and analysing leachates from the soil column, it is possible to derive information about interactions of the test substance with soil constituents. Column leaching tests are increasingly applied in studies on nanoparticle behaviour in order to determine kinetic transport parameters introduced in section 2.4 (He et al., 2019; Jiang et al., 2012; Rahmatpour et al., 2018; Raychoudhury et al., 2010).

3.4.1 Column experiment design

Transport of nanoplastics by water through soil was studied using a glass column filled with disturbed saturated soil connected to a bottom-up water flow powered by a peristaltic pump. Thereafter, leachate from the column passed through a flow meter (Truflow, Glass Expansion) and a conductivity meter (Conductivity isoPod, EPU357) before reaching a fraction collector. A schematic design is presented in Figure 5. The design was based on OECD guidelines (2004), with a protocol adjusted by Cornelis et al. (2018) for nanoparticle transport natural soils.

Concentrations in leachate were measured for obtaining breakthrough curves and the retained particles in the soil for determining the spatial distribution in retention profiles.

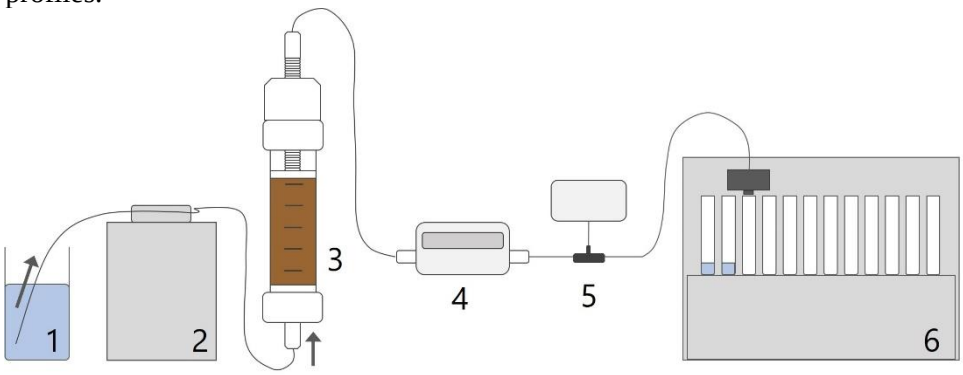

Figure 5: Experimental setup for investigating advective transport of nanoplastics in soil columns. Schematic design including: 1) injected solutions, 2) peristaltic pump, 3) soil-filled glass column with bottom-up flow, 4) flow meter, 5) conductivity meter with a flow-thru conductivity electrode and 6) fraction collector. Arrows indicate the direction of flow.

Experiment setup of column tests

The Omnifit glass column measured 10 cm total, with a maximum 7 cm effective inner length and a 2.5 cm inner diameter. Tube fittings at each end were fixed by caps, with one adjustable tube fitting. At each end of the column, Nylon-filters of 70 µm mesh size (Spectra/Mesh) were inserted to prevent displacement of larger particles into tubes while still allowing colloids and nanoplastics to pass. The column was wet filled by successively adding small amounts of artificial rainwater and soil to the column, ensuring saturation of the soil by an excess of water. Entrapment of air was minimized by tapping the column after each addition of soil until no air bubbles were rising. Soil was oven-dried at 105°C for 24 hours prior to column packing. Artificial rainwater was prepared from salts dissolved in ultrapure water, i.e. sodium chloride, sodium nitrate, calcium chloride and ammonium sulphate (Supplementary Table S6). The total porosity and soil bulk density of the packed columns were estimated from the dimensions of the packed columns and the added masses of water and soil. Liquid lost from the column during closing of the column was collected and accounted for during mass calculations. The estimated pore volume (mL) was defined as the amount of water added to the column during packing. The column experiment was conducted in several steps: stabilization, inert tracer pulse, nanoplastic suspension pulse, collection of leachates followed by Pd-detection. First, for ensuring stable conditions in terms of flow and conductivity, the column was leached with particle-free artificial rainwater for at least four pore volumes at mean flow rates of approximately 8.15×10^{-2} cm s^{-1}. After a quasi-steady-state flow regime was reached, an inert tracer (10 mM $NaNO_3$) was injected for approximately two pore volumes, followed by at least two pore volumes of artificial rainwater to return to baseline conductivity. Conductivity was used to obtain a breakthrough curve for the pulse of the inert tracer. Thereafter, a pulse of nanoplastics of 1 mg L^{-1} suspended in artificial rainwater was injected (2.4 µg Pd L^{-1}). The

suspension was prepared within 1 h before the measurement. Another four pore volumes of particle-free artificial rainwater were applied. The flow rate was maintained at approximately 8.15×10^{-2} cm s^{-1} throughout the whole procedure. With the onset of the injection of the spiked solution until the end of the experiment, leachates from the column were collected using a fraction collector at intervals of 5 minutes. In the final step, the Pd-concentrations in the effluent was measured (section 3.3). Figure 6 provides a simplified overview of data acquisition and processing steps undertaken for the column experiment.

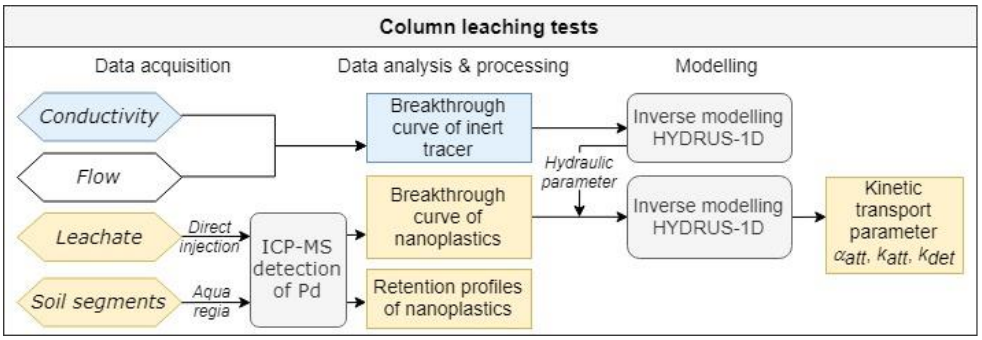

Figure 6: Simplified overview of data acquisition, processing and modelling steps for leachates and soil segments from advective transport tests in soil columns with Pd-doped nanoplastics.

3.4.2 Acquisition and processing of leachate and soil profile data

Soil column leachate

The leachates collected by the autosampler were injected directly into the ICP-MS for measuring the Pd-concentrations. For optimizing matrix matching, solutions with known Pd-concentrations were prepared in three different media: 3 % HCl, ultrapure water and effluent from one of the soil columns. The detected raw intensities were corrected by the ICP-MS operating software, providing net intensities corrected using the indium standard. Net intensities were then used to produce calibration curves for each dilution medium, displayed in Figure 7. In general, net intensities associated with the same Pd-concentration differ substantially between dilution media with lower net intensities detected in ultrapure water and column effluent as opposed to standards prepared in 3 vol.% HCl. Palladium concentrations calculated using a calibration curve from standards prepared in 3 vol.% HCl are therefore likely an underestimate of actual concentrations if the matrix of the samples corresponds more to ultrapure water. This has to be taken into consideration when detecting palladium incorporated into particles in soil leachates. Similarly, concentrations calculated using the effluent-based calibration are likely to overestimate Pd-concentrations. Other ions and dissolved molecules that dissolved Pd interacts with may be present in effluents from the soil columns, whereas particle-incorporated Pd remains unaffected. Therefore, Pd-concentrations in soil column

leachates were first determined based on the calibrations using HCl-standards, and afterwards converted to the corresponding calibration curve in ultrapure water measured at the same time as each leachate set. Based on the detected concentrations of nanoplastics in the leachate, a time-dependent breakthrough curve could be obtained for each column experiment by synchronizing flow data with sampling times and detected Pd-concentrations in the samples.

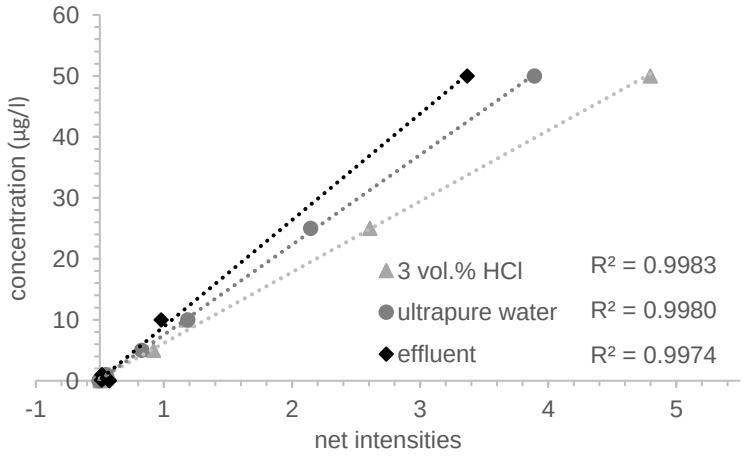

Figure 7: Calibration curves for ICP-MS detection of palladium for different matrices: 3 % HCl, ultrapure water and effluent from soil columns used for transport studies. Net intensities are corrected for blank measurements and internal In-standards.

Soil segments

The spatial distribution of retained particles in the soil profile was investigated by segmenting the soil as a function of depth and measuring the total Pd concentrations in each segment after microwave-assisted *aqua regia* digestion. The soil was cut into approximately 0.5 cm thick segments with a metal spatula while pressing it out of the column over the adjustable tube fit. The wet weight of each segment was measured, and traces of soil or water rinsed off the spatula into the same beaker. Glass beakers were all previously acid-bath washed, rinsed with ultrapure water and dried. The soil segments were oven-dried at 50°C for three days. Dry samples were weighed, homogenized using an agate mortar, and then prepared for microwave-assisted digestion as described above (section 3.3.2). The resulting Pd-concentrations were corrected for the background concentration in the soil (32 µg kg^{-1}) to produce depth profiles of retained nanoplastics. Statistical significance was tested by one-way ANOVA and post-hoc Bonferroni tests ($p<0.05$) for examining the differences of detected Pd-concentrations to background concentrations.

Recovery of nanoplastics in leachate and soil

For each soil column experiment, a nanoplastic mass balance was conducted using the Pd-concentrations in effluent and from particles retained in the soil. Thereby, the sum of the measured mass in both leachates and soil fractions was calculated and compared to the total amount of injected mass over the experiment duration.

The injected mass could be estimated based on concentration in suspension, injection time and flow rate.

3.4.3 Modelling particle mobility using HYDRUS-1D

For modelling of nanoplastic transport in saturated soil columns the presented advection-reaction-dispersion (ARD) equations were applied for simulating one-dimensional movement of solutes and particles. In a first step, data from the experimental inert tracer breakthrough curves (BTC) was utilized to estimate transport parameters of the bulk solution, i.e. longitudinal dispersivity and effective porosity. This was done by applying the ARD equation for solute transport (Equation 1) in an inverse modelling approach using the advanced iterative model HYDRUS-1D. The derived hydraulic parameters were thereafter implemented in a second inverse model in order to obtain kinetic transport parameters from nanoplastic BTCs.
Following an approach by Bradford et al. (2003), two model approaches considering different potential interactions were applied in HYDRUS-1D: 1) attachment only (M1) and 2) attachment and detachment (M2). For this purpose, the ARD equation for colloid transport (Equation 2, 3) was applied to determine attachment rate coefficient (k_{att}), attachment efficiency (α_{att}) and detachment rate coefficient (k_{det}). Underlying assumptions were a two-phase liquid-solid system, i.e. a soil with fully saturated pore system, a physical equilibrium in terms of hydraulic conditions, such as steady-state homogeneous flow, and completely kinetically controlled interactions of nanoplastics with the surfaces of the bulk soil.
Simulation conditions for parameterization of the model comprised a mean collector diameter (d_{50}) of 155 µm and a nanoplastic diameter of 256 nm. Soil depth, dry bulk density, initial estimates for porosity and mean linear flow velocity were determined for each column separately based on experimental conditions. Hydraulic conductivity and retention parameters were determined by applying Rosetta DLL for solving pedotransfer functions via neural network predictions from texture class information (Table 1) and dry bulk density (Schaap et al., 2001). In some cases, effective porosities obtained from the tracer BTCs were re-calibrated manually for the nanoplastic BTCs for achieving better fit. The model fit was evaluated based on the R^2 of the regression of predicted against observed effluent concentrations.

3.5 Bioturbation study

3.5.1 Bioturbation experiment design

The transport of nanoplastics by bioturbation was investigated in microcosm tests by introducing *Lumbricus terrestris* to soil-filled plots of ca. 30 cm length including a ca. 2 cm soil layer at the top spiked with Pd-doped nanoplastics. Over a period of four weeks, the spatial distribution of particles within soil profiles was analysed by sampling in weekly intervals. Soils segments were investigated with regards to their Pd-content to determine the impact of bioturbation on nanoplastic redistribution.

Species selection and characterization of individuals

The selection of *Lumbricus terrestris*, an anecic species, for the bioturbation study was due to its potential for high bioturbation intensity over short time-scales due to its deep-burrowing behaviour and preferred vertical movement in soils. The deep burrows of *L. terrestris* are partly permanent (Blume et al., 2016).
Adult individuals of *L. terrestris* were purchased from an external supplier (Wormsdirect, UK) and stored for one week for acclimatization before the onset of the experiment. For determining length and wet weight, individuals were rinsed with cold water, separately placed into petri dishes with wet filter paper to maintain hydration status and kept in the dark at 13°C for 48 h. Casts were regularly removed to ensure complete depuration. Preparation steps and characterisation followed recommendations by Fründ et al. (2010). Individuals were then introduced to the columns by random selection. A stocking density of three worms per column was selected in order to ensure sufficient bioturbation activity during the available time. Corresponding to 382 individuals m^{-2}, this density is higher than the typical ranges found in most land uses/land covers, but according to Fründ et al. (2010) is not uncommon for temperate pastures.

Setup of bioturbation experiment

Cylindrical polyvinyl chloride (PVC) plots of 10 cm diameter, 35 cm total length were packed with 28 cm of untreated soil, overlain by 2 cm of spiked soil and an artificial litter layer as depicted in Figure 8A. At the beginning of the experiment, 4 g *Tilia* leaves, oven-dried at 70°C, were added to each column. Another 2 g were added after two weeks, and another 1 g after three weeks to maintain a litter layer at the surface. Below the in total 30 cm thick soil layer, a 1 cm thick layer of sand allowed for free drainage of the column to avoid saturation, which has been previously shown to induce avoidance patterns of earthworms (Baccaro et al., 2019). The bottom of the plot was closed off with a 1 mm aluminium mesh, and the top with a 1 mm glassfiber mesh. This allowed for drainage and aeration while keeping the soil in place and preventing earthworms from escaping. In order to achieve an even distribution of moisture at the onset of the experiment, the soil was brought to a water content of approximately 16.8 % w/w before packing, corresponding to 40 % of its water holding capacity. Weight of wet soil added was noted for each plot and initial dry bulk density calculated. The moisture content during the experiment was maintained by regular weighing and spraying application of deionized water (2-3 times $week^{-1}$). Similar compactness of the soil was achieved by tapping the column on the table for an equal amount of times after packing. The plots were kept in the growth chamber (Figure 8B) for four days and spiked soil was added 2 h before the onset of the experiment. The initial Pd-concentration in the spiked layer was 26 mg kg^{-1}. For each plot, this corresponded to a total of 588 mg particles, or 3.91 mg palladium in the spiked layer. In total, 15 plots with spikes were prepared. Twelve of these included treatments with earthworms covering four sampling timepoints with three replicate columns each. The remaining replicate set was kept as control spiked with nanoplastics but without earthworms analysed after four weeks. Moisture was also maintained for control plots. In the growth chamber the columns were arranged in a semi-random block system as shown in Figure 8B to account for potential

differences in micro-climate depending on placement. The bioturbation and control plots were exposed to daylight (24 h) over the entire duration of the experiment, with a relative humidity of 60 % and temperatures of 13°C in the growth chamber.

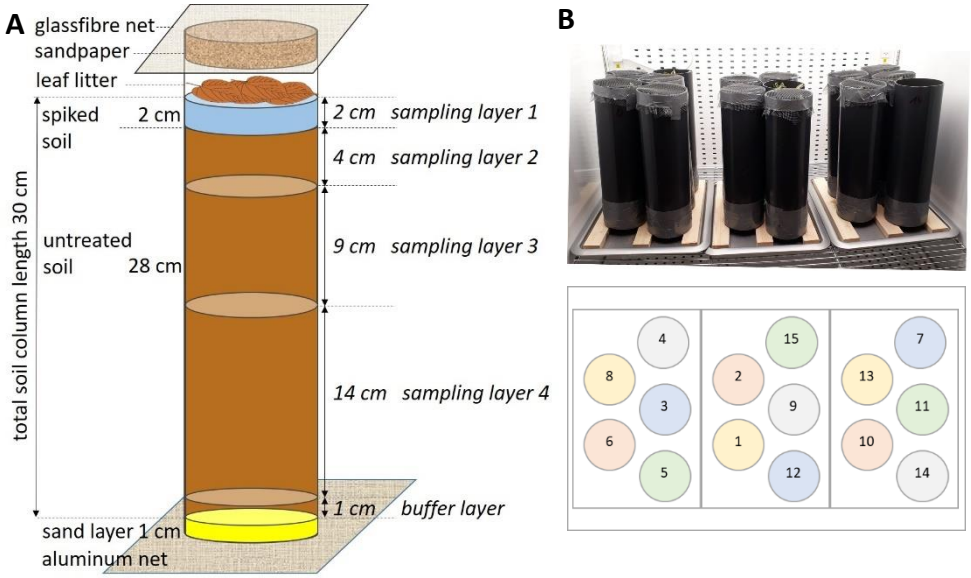

Figure 8: Overview of bioturbation plot setup and arrangement in the growth chamber. A) Setup and segmentation for analysis. B) Arrangement of columns in growth chamber with a semi-random block system, colours indicate replicates of one batch treated with the same spiked soil.

3.5.2 Acquisition and processing of data from bioturbation plots

Samples were taken weekly, starting with the first timepoint seven days after introduction of the earthworms, then repeatedly after 14, 21 and 28 days. The intact soil plot was successively pressed out of the PVC container, followed by depth-based segmentation and homogenization of the separate layers. Thereby, the soil core was divided into four layers: 0.0-2.0 cm, 2.0-6.0 cm, 6.0-15.0 cm and 15.0-29.0 cm (Figure 8A). At the bottom 1 cm of soil was discarded together with the sand layer to avoid dilution. The higher resolution of sampling layers at the top was chosen as changes were expected to occur over shorter timespans with Pd-concentrations above detection limit, providing reliable data for modelling. The sampling scheme further aimed at avoiding hotpot detection and reduce challenges in accurately sampling distinct layers as has been found problematic by Baccaro et al. (2019). After oven-drying at 105°C for at least three days, dry weight was noted. The soil for each sampling layer was then ground and homogenized by mechanic sieving, remaining aggregates manually ground in a mortar and particles over 2 mm removed. For ensuring representative samples, subsamples were taken by dividing the total sample into halves in multiple steps, except for timepoint 1. The mean concentration per sampling layer was then measured based on triplicate subsamples treated according to the microwave-assisted digestion protocol (section 3.3.2). The general Pd-background concentration of the soil established during material characterization

(section 3.1) was used as a baseline reference. Detected Pd-concentrations in the extracts were corrected for this background. The water content for each layer was measured after sampling. The earthworms were carefully removed during the disintegration of the soil segments and prepared for depuration as described above. In order to assess potential negative impacts of the experimental setup or exposure to plastics, changes in depurated fresh weight and length were documented.

Statistical analysis and recovery of nanoplastics

Kolmogorov-Smirnov tests were conducted for testing normal distribution of data per layer, containing all replicate plot subsamples of the particular layer (n = 9). The statistical significance of differences in detected concentrations was tested by one-way ANOVA and post-hoc Bonferroni tests (t-test, same variance) at significant levels of $p<0.05$. Recovery of palladium from soil was estimated in a mass balance based on total added Pd, detected concentrations and corresponding weight.

3.5.3 Modelling nanoplastic transport by bioturbation

Modelling of nanoplastic transport by bioturbation followed an approach applied by Baccaro et al. (2019), implementing the bioturbation model developed by Rodriguez (2006) and explained in section 2.6. The bioturbation rate ($k_{bioturb}$) was determined by adjusting the bioturbation fitting parameter β and solving Equation 8 to obtain predicted concentrations close to experimental data using the sum of squared errors calculated on logarithmic concentrations as a measure of fit.
The earthworm density and volume of the column were set according to experiment conditions (section 3.5.1). As palladium was used for detection, models were based on the detected Pd-concentration, while results are reflecting the fate of the nanoplastics. The bioturbation column was segmented into 29 layers of depth d_l = 0.01 m each with an associated simulated Pd-concentration. Thereof, the initial spike concentration 26.1 mg kg^{-1} was assigned to the first two layers of depth d_l. Accordingly, the Pd-concentration for each underlying layer was calculated at a specific time after the onset by applying Equation 8. Days used as timestep to allow for comparison with the experimental data obtained after 7, 14, 21 and 28 days. The mean concentration of the sampling layers (Figure 8) were predicted by taking the mean of all modelled depth layers d_l corresponding to the thickness of the particular sampling layer. The relative model fit was determined by using the R^2 of the regression of simulated against observed Pd-concentrations in the different sampling layers at the specific timepoints. Afterwards, the time span until complete mixing was calculated.

4 Results

4.1 Column transport studies

In total four leaching experiments were conducted to determine nanoplastic mobility via advective transport, comprising one replicate column of 3.70 cm length (R1) and three replicate columns of lengths between 6.9-7.0 cm (R2-R4). The dry bulk density, measured porosity and mean linear velocity varied between the replicates (Table 3). Compression in deeper parts of the profile, i.e. near the outflow, with higher bulk densities was noted for R3 and R4, that are associated with the closing of the column (Supplementary Figure S1).

4.1.1 Soil column depth profiles of retained nanoplastics

The soil columns were analysed for retained particles based on Pd-concentrations as described in section 3. The resulting retention profiles for each column are shown in Figure 9, following the direction of flow with depth increasing from the inlet. At the given inlet particle concentration of 1 mg L^{-1}, or 2.4 µg Pd L^{-1}, no distinctive pattern was observed in the retention profiles among the four replicate columns (Figure 9). Challenges were encountered with regards to detection limits as indicated by negative values obtained after corrections for Pd-background concentrations in the soil. In some instances, significant differences ($p<0.05$) between detected and background Pd-concentrations could be observed. Retained nanoplastics detected in R3 followed no depth-dependent trend, whereas in R4 these were concentrated in the lower parts of the profile. Only for the short column (R1) could nanoplastics be found throughout the entire column, with increasing retention with depth.

Table 3: Summary of column-specific soil properties, experimental conditions and recovery of injected particles in measurements, based on detected Pd-concentrations in leachate and retained in soil. Recovery in soil was re-calculated (in parentheses) based on correction factors suggested by Bradford et al. (2004).

Column			R1	R2	R3	R4
Length of column	x	*(cm)*	3.7	6.95	7.00	6.90
Bulk density	ρ_b	*(g cm-³)*	1.19	1.27	1.28	1.40
Measured porosity	θ	*(%)*	50%	52%	50%	45%
Mean linear velocity	v	*(cm min^{-1})*	0.175	0.150	0.146	0.146
pH	*pH*				7.2-7.6	
Particle concentration (at inlet)	C_0	*(mg L^{-1})*			1	
Mean particle diameter medium	d_{50}	*(µm)*			155	
Density of nanoplastics	ρ_p	*(g cm-³)*			1.05	
Z-average diameter of nanoplastics		*(nm)*			256.1	
Recovery effluent$_{\text{ultrapure water}}$		*(%)*	97	66	194	79
Recovery effluent$_{\text{3% HCl}}$		*(%)*	79	57	73	56
Recovery in soil$_{\text{non-corrected}}$		*(%)*	197 (3)	66 (34)	218 (-)	648 (21)

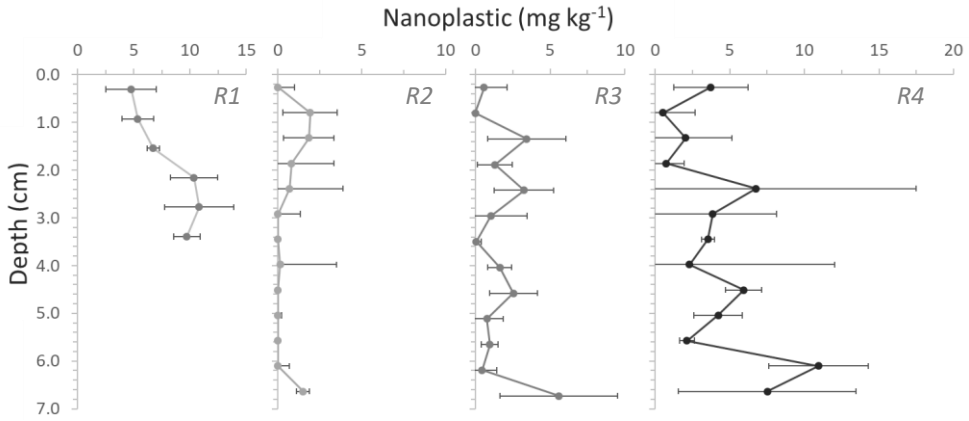

Figure 9: Retention profiles of soil columns showing retention of Pd-doped nanoplastics (mg kg^{-1}) in relation to depth based on detected Pd-concentrations from leaching experiments at inlet concentrations of 1 mg L^{-1}. Replicates from left to right R1-R4.

4.1.2 Tracer breakthrough curves and derived hydraulic properties

Breakthrough curves (BTCs) were obtained for all replicate soil columns, describing the change in concentrations of tracer and nanoplastics detected in effluent as a function of time expressed in terms of the number of eluted pore volumes (Supplementary Figure S2). Normalized concentrations were used, defined as the effluent concentration C divided by the influent concentration C_0. In all cases, absence of interactions of the tracer substance ($NaNO_3$) with the soil constituents was confirmed, as the tracer substance was fully recovered. Concentrations at the peak were equal to influent concentrations C_0. Thus, tracer BTCs were considered representative for the movement of pore fluid through the columns and utilized to determine

hydraulic properties. Longitudinal dispersion of the soil pore water and effective porosity were obtained by inverse modelling of the experimental data in HYDRUS-1D. Notably, values for effective porosity derived during inverse modelling were very low, ranging from 18-21 % as opposed to initial estimates (45-52 %) (Table 3 and Table 4). Although the same protocol had been applied for packing, longitudinal dispersivity and effective porosity obtained by inverse modelling also differed between replicates (Table 4). The overall fits for the tracer models generated by inverse modelling in HYDRUS-1D were good, expressed in an R^2 above 0.98 of the regression of predicted against observed data (Supplementary Table S7). The resulting longitudinal dispersivity ranged from 1.2×10^{-7} m^2 s^{-1} to 7.7×10^{-7} m^2 s^{-1}, at modelled water contents of 18-20 % (Table 4). Replicate 2 and 3 showed stable conditions with relatively symmetrical BTCs, a stable plateau and only minor tailing. Conversely, BTCs of R1 and R4 were slightly skewed, with a decreasing slope steepness in the front towards the exhaustion point (C/C_0 = 0.95) and more pronounced tailing. Irrespective of the modelling approach, R1 and R4 displayed higher longitudinal dispersivity than the other two replicates (Table 4). Considering that the same protocol was applied for all columns and no systematic difference between R1 and R4 to R2 and R3 is apparent based on the experimental conditions listed in Table 3, variations may have been introduced while packing.

4.1.3 Experimental and modelled breakthrough curves of nanoplastic transport studies and attachment efficiencies

Due to variations observed in the nanoplastic BTCs between the replicate soil columns, each replicate is presented separately with corresponding simulations to show the fit of applied models (Figure 10). As compared to the overall movement of the bulk solution, represented by the tracer data, four trends were observed for the BTCs of the raspberry-shell polystyrene nanoplastics: 1) the breaking point was reached faster for nanoplastics than for the tracer (R1, R3, R4), 2) in most cases the influent nanoplastic concentration C_0 was not fully detected at the peak, even after a plateau was established (R2-R4), 3) in one case a narrow secondary peak developed after establishment of a plateau (R2) and 4) tailing was more pronounced (R1-R4). The only case in which the injected nanoplastic was almost entirely recovered in the effluent was in the short column (R1). Note that the recovery potential of direct injection was previously found to correspond to 90-95 % of the actual concentration (section 3.3.4). Columns with multiple peaks also showed minor fluctuations prior to the development of the secondary peak (R2-R4) that were not present in the tracer BTCs. In one case a tertiary narrow peak developed during decline (R4), and in two cases another narrow peak developed during the tailing (R3, R4). Obtained values of higher longitudinal dispersivity were associated with stronger tailing for nanoplastic BTCs (R1, R4). The water content of the HYDRUS-1D model had to be recalibrated manually to the BTC of nanoplastics (R1-R4) in order to yield the model fits displayed in Figure 10. The recalibrated effective porosities were lower than values obtained from the tracer BTCs and are displayed in Table 4.

Overall, the raspberry-shell PS-nanoplastics showed a high mobility in saturated soil columns as most of the injected particles could be recovered in the effluent.

Accordingly, attachment efficiencies derived from HYDRUS-1D were low (Table 4). For both models, attachment only (M1) and attachment-detachment (M2), values ranged from $\alpha_{att} = 2.8 \times 10^{-4}$ to $\alpha_{att} = 1.0 \times 10^{-3}$. Attachment rate efficiencies of three replicates were only marginally higher when including detachment in the model (M2).

Overall, the applied models were able to predict nanoplastic transport with good fits of simulated to experimental data, expressed in an $R^2 = 0.96$ to $R^2 = 0.99$ (Supplementary Table S7). In general, the model considering only attachment (M1) yielded marginally better fits. Despite good fits, both models were not able to adequately simulate the multiple narrow peaks observed in the experimental data. Including detachment (M2) resulted in slightly improved fits for R3, but was not able to reflect secondary or tertiary peaks. Simulating detachment generated BTCs with either slightly higher concentrations in the plateau phase (R2) or with increased tailing (R3, R4). Derived detachment rate coefficients were at least one order of magnitude lower than attachment rate coefficients (Table 4). Detachment was thus occurring at a slower rate than attachment. One exception is R1, where the derived detachment rate coefficient was similar to the corresponding attachment rate coefficient.

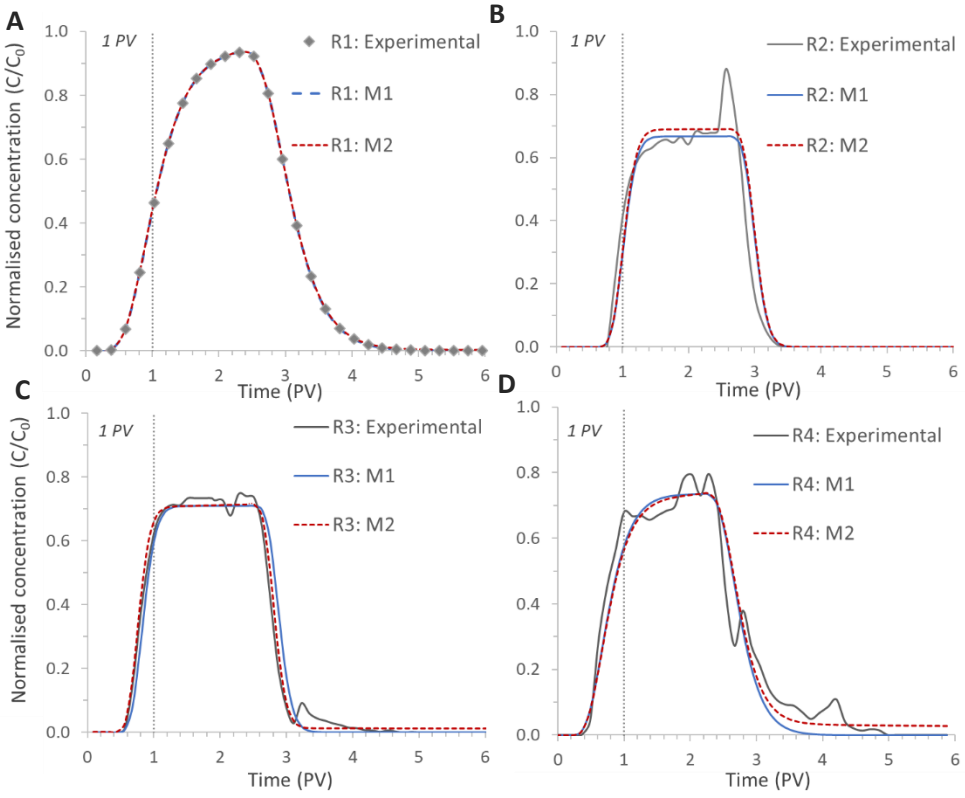

Figure 10: Breakthrough curves with normalized concentrations for four replicate column leaching studies on advective transport of nanoplastics in a natural soil. Presented are measured and simulated values, based on two models implemented in HYDRUS-1D with M1 for attachment only and M2 for attachment and detachment. A) Replicate 1, 3.7 cm length, B) Replicate 2, 6.9 cm length, C) Replicate 3, 7.0 cm length and D) Replicate 4, 6.95 cm length.

Table 4: Particle transport parameters derived from manual fitting and inverse modelling in HYDRUS-1D. M0: Effective porosity and longitudinal dispersivity obtained from tracer data. Effective porosity was recalibrated for nanoplastic BTCs ( ). M1: Attachment only model. M2: Attachment and detachment model.

	Column			R1	R2	R3	R4
M0	Effective porosity	θ	*(%)*	18 (15)	20 (14)	21 (10)	19 (10)
	Longitudinal dispersion coefficient	D_L	*($m^2\ s^{-1}$)*	4.5×10^{-7}	1.2×10^{-7}	1.7×10^{-7}	7.7×10^{-7}
M1	Attachment rate coefficient	k_{att}	*(s^{-1})*	3.3×10^{-5}	1.4×10^{-4}	1.5×10^{-4}	1.6×10^{-4}
	Attachment efficiency	a_{att}		2.8×10^{-4}	1.0×10^{-3}	6.5×10^{-4}	5.7×10^{-4}
M2	Attachment rate coefficient	k_{att}	*(s^{-1})*	3.5×10^{-5}	1.4×10^{-4}	1.7×10^{-4}	1.7×10^{-4}
	Detachment rate coefficient	k_{det}	*(s^{-1})*	2.9×10^{-5}	6.9×10^{-7}	9.2×10^{-6}	3.3×10^{-5}
	Attachment efficiency	a_{att}		2.8×10^{-4}	1.0×10^{-3}	6.7×10^{-4}	6.6×10^{-4}

4.1.4 Recovery of injected plastics

Nanoplastic recovery in the leachate of the replicates was high, ranging between 66-194 % of the total injected mass (Table 3), based on calibrations in ultrapure water. For the soil columns, the particle mass was calculated for each segment resulting in a strong overestimation for R1, R3 and R4 (197-648 %). Due to challenges with detection limits in soil samples and the expected higher error during sample preparation for acid extraction, effluent recoveries were considered more reliable. For the total mass balance, the difference between recovered mass in leachates and total injected mass was considered retained nanoplastics in accordance with the correction factor suggested by Bradford et al. (2004).

4.2 Bioturbation studies

4.2.1 Worm fitness and burrowing behaviour

The change in mean earthworm weight and length before and after the experiments were compared for each plot and sampling point as an indicator for worm fitness. The observed changes in mean earthworm weight were found non-significant ($p>0.05$) (Supplementary Table S8). Burrows were found throughout the transect of plots during sampling, indicating that movement, thus bioturbation, occurred throughout the transect and not exclusively at the edges (Figure 11).

4.2.2 Water application, soil moisture and experimental conditions

In order to maintain the soil moisture, water was added to bioturbation and control plots 2-3 times per week depending on observed water loss (Supplementary Table S9). On average, water applications corresponded to a rainfall intensity of

8.2 mm week^{-1}, with approximately 3.7 ± 0.6 mm per application. The water content of the soil at sampling corresponded to approximately 43 % of the water holding capacity. This was the case for all layers and timepoints, except the lowest layer where water contents were significantly lower ($p<0.05$) around 35 %, in bioturbation and control plots respectively. No water loss through drainage was observed. The general recovery of the spiked material ranged between 64-74 % of the added 3.91 mg per column (0.59 g plastics). Note that previously in the presence of soil approximately 91 % of plastic-incorporated Pd was recovered (section 3.3.4). At the last timepoint, the detected concentrations in the lower two layers were based on a reduced replicate set due to deviations from the sampling protocol (section 3.5.2).

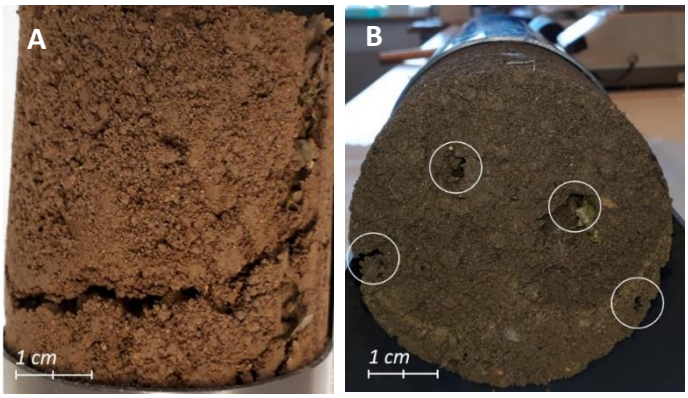

Figure 11: Documentation of burrowing behaviour of L. terrestris in bioturbation plots. A) Burrows along the sides of the column observed after one week. B) Burrows (highlighted in white) along the sides of column and in the centre of the transect after two weeks.

4.2.3 Temporal changes of spatial particle distribution

Nanoplastic concentrations in the bioturbation experiment were indirectly measured through Pd-concentrations. Bioturbation plots were analysed weekly over the total duration of four weeks (T1-T4), with three replicates at each sampling point that were segmented into four layers (L1-L4). In order to ensure detectability of change in Pd-concentrations throughout soil profiles of the plots exposed to bioturbation, the differences in concentrations of adjacent layers were analysed separately for each replicate at each timepoint. Differences between adjacent layers in the same column were found significant in all cases ($p<0.05$), including control plots.
Three general trends were observed with regards to the spatial distribution of particles in the bioturbation plots: 1) the highest concentrations were exclusively found in the uppermost sampling layer, 2) concentrations within each plot decreased with depth, and 3) over time concentration decreased in the uppermost sampling layer and increased in the lower parts of the profile. Nanoplastic concentrations in the third and fourth layers were consistently increasing over the whole duration of the experiment, and significantly during the first three weeks (Figure 12). Notably, the largest change occurred between the second and third sampling timepoint (T2-T3) and were less pronounced between week three and four (T3-T4).

The bioturbation plots were supplemented by control plots (C), that were subjected to water addition only and sampled after four weeks. In the control plots, the detected Pd-concentrations of the lower two sampling layers were not significantly different ($p>0.05$) from the background concentrations of the soil (Supplementary Table S10). Consequently, without bioturbation no nanoplastics could be detected in the lower two layers under water additions corresponding to 8.2 mm week^{-1}.

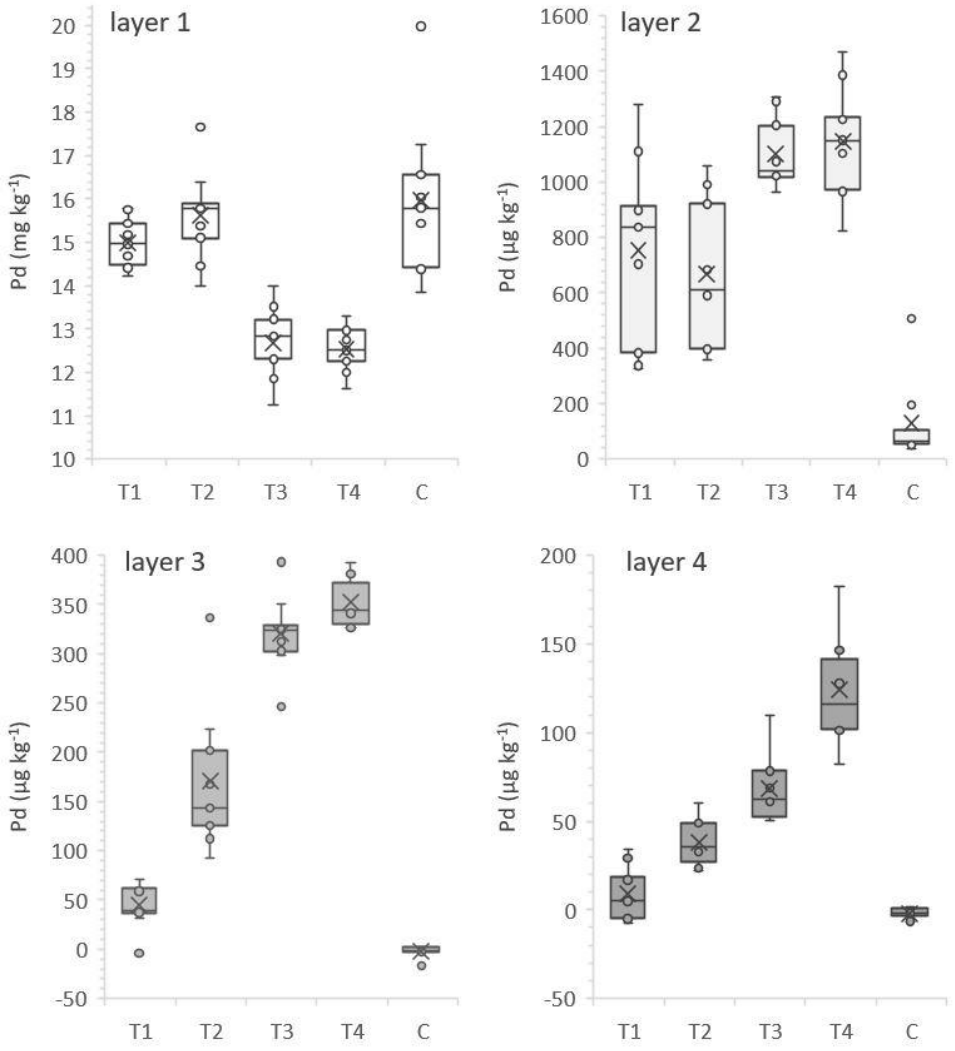

Figure 12: Detected Pd-concentrations as approximation for nanoplastic at different depths in soil profiles after different time spans of exposure to bioturbation. Layers correspond to depths of 0.0-2.0 cm (L1), 2.0-6.0 cm (L2), 6.0-15.0 cm (L3) and 15.0-29.0 cm (L4). Samples were taken weekly (T1-T4) over a total of 4 weeks. Box plots represent the distribution of the first to third percentile, bars display variation, points datapoints. The cross marks the mean of the distribution. Results are based on ICP-MS measurements of aqua regia digested soil samples, with triplicate plots and triplicate soil samples per layer. Note that the sample set was reduced for L3 and L4 at T4 (6 replicates instead of 9).

4.2.4 Bioturbation rates for modelling the biologically mediated transport of nanoplastics

The bioturbation rate ($k_{bioturb}$) was determined by adjusting the bioturbation fitting parameter to fit the experimental data. Logarithmic concentrations were used for fitting in order to increase the sensitivity of the model to the deeper soil profile in which plastic concentrations were lower. Different fits of the bioturbation model are shown in Figure 13 with corresponding parameters displayed in Table 5.

When considering all layers equally for fitting of the model to experimental data (Figure 13A), the resulting bioturbation fitting parameter $\beta = 4.50 \times 10^{-11}$ m^4 s^{-1} at a depth step of $d_l = 0.01$ m yielded a bioturbation rate of $k_{bioturb} = 5.7 \times 10^{-6}$ s^{-1}. While obtaining the lowest overall error, the potential in predicting the concentrations as a function of time based on this bioturbation rate differed substantially between layers (Figure 13A). In particular, predicting the concentrations of the fourth and thickest sampling layer imposed some challenges. When adjusted to layers closer to the surface, the model systematically underestimated concentrations in the lower soil profile. Conversely, when fitting the model to the lower two layers, the concentrations in the second layer were largely overestimated. By down-prioritizing the lowest layer, predictions were improved for layer 1 and 3 displayed in Figure 13B. This was justified given the large thickness of the sampling layer. The corresponding $\beta = 2.30 \times 10^{-11}$ m^4 s^{-1} resulted in a bioturbation rate of $k_{bioturb} = 2.9 \times 10^{-6}$ s^{-1} ($d_l = 0.01$). The relative fit of the models was expressed in R^2 (Supplementary Figure S3).

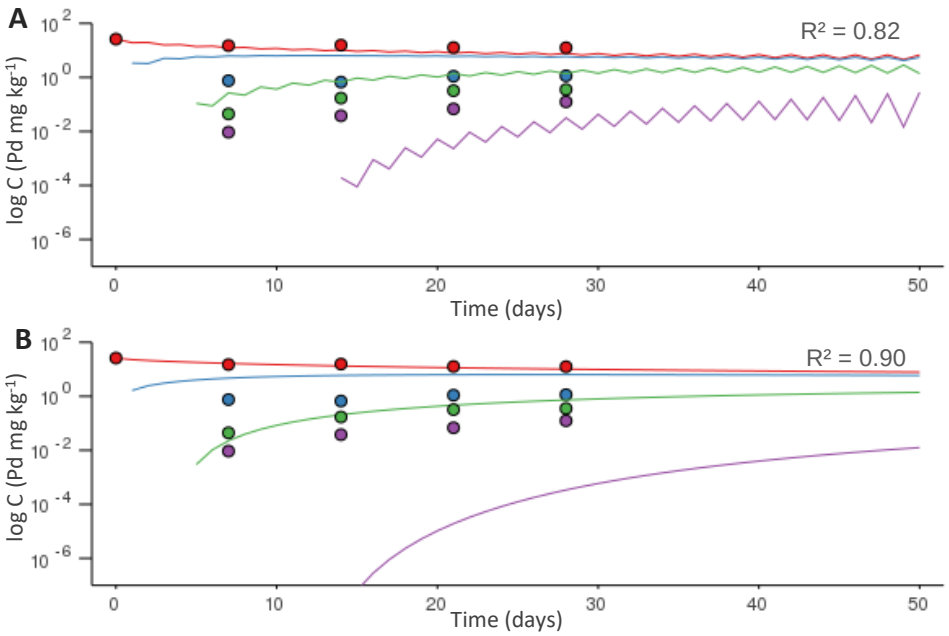

Figure 13: Changes in mean concentrations of Pd-doped plastics in different soil layers over time as a result of transport by bioturbation. Measured (points) and simulated (lines) Pd-concentrations for layer 1 (red), layer 2 (blue), layer 3 (green), layer 4 (purple). The model fit is described by R^2 of the regression of simulated versus experimental data. Parameters are valid similarly for nanoplastics. A: Model fit to all layers (L1-L4). B: Model fit to L1-L3.

Table 5: Bioturbation rate and corresponding fitting parameter determined for bioturbation plots exposed for 4 weeks. The bioturbation model was fit by obtaining least sum of squares of logarithmic simulated to measured concentrations.

	$k_{bioturb}$ (s^{-1})	β ($m^4\ s^{-1}$)	R^2
Figure 13A	5.7×10^{-6}	4.50×10^{-11}	0.82
Figure 13B	2.9×10^{-6}	2.30×10^{-11}	0.90

For estimating complete mixing, estimated concentrations of each layer of depth d_l (n = 29) were considered. According to bioturbation rates of the two models (Figure 13A and 13B), complete mixing was reached after 628 days or 997 days, so two to three years under unchanged experimental conditions.

5 Discussion

Overall, in water-saturated soil columns, polystyrene nanoplastics were highly mobile with only very limited attachment occurring during advection. Conversely, nanoplastic mobility was limited if particles were present in unsaturated soils that were repeatedly subject to water addition and subsequent periods of drying as was the case for control plots of the bioturbation study. Despite limited advection-driven transport occurring at variable water contents, displacement of nanoplastics still occurred due to bioturbation activities of burrowing soil biota, here by the earthworm *Lumbricus terrestris*. Natural soils are subject to precipitation and percolating water, as well as drying and movement of soil biota causing biologically mediated displacements. With respect to field conditions, it is more likely that variable moisture contents predominate so that the unsaturated control plots of the bioturbation experiments are more representative compared to the saturated soil columns. In the experiments conducted in this study, it was possible to derive transport parameters useful for predicting nanoplastic transport in soils.

Nanoplastic transport in soils by advection

The raspberry-shell polystyrene nanoplastics used in this study were highly mobile in water-saturated soil pore systems under the influence of advection as compared to other studies on nanoparticle transport (Li et al., 2019; Torrent et al., 2019). The overall low affinity of the nanoplastics for the soil was reflected in high recoveries in the soil column leachate and subsequently derived kinetic transport parameters based on breakthrough curves. By determining and applying kinetic parameters in transport models, it was possible to predict the mobility of the used polystyrene nanoplastics over a certain transport distance in a particular soil. The mean attachment efficiency of nanoplastics, $\alpha_{att} = 6.25 \times 10^{-4}$, was derived from four replicates. This first insight draws attention to potential long-term risks, such as leaching of particles to greater depths in soils, groundwater bodies and freshwater or marine environments. In order to reliably assess potential risks, it is important to understand the underlying processes that determine nanoplastics fate in soils.

The PS-nanoplastics used in this study were characterized by a high negative zeta potential and suspensions remained stable in soil column leachates. According to DLVO theory, positively charged sites were expected to be preferred sites for attachment and interactions (Elimelech et al., 1995). This comprises Al- and Fe-(hydr)oxides, with an expected positive net surface charge at the pH range of the

used soil (Essington, 2004). Considering the relative hydrophobicity of many plastics and the high affinity of organic contaminants for polystyrene reported by Lee et al. (2014), interactions were also expected with organic substances present in the soil. With 2.5 % w/w of organic carbon in the soil, the organic matter content was representative for agriculturally used soils (Wiesmeier et al., 2012). Opposed to expectations experimental data showed low retention and corresponding low attachment efficiencies.

Reasons for this could be related to soil or nanoplastic properties. For once, at high pH of the pore water Fujita and Kobayashi (2016) reported strong negative charges of silica and sand causing strong repulsion of nanoparticles. As these are expected to constitute the main proportion of the soil particles, strong repulsion of the nanoplastics under the present pH is likely to inhibit potential interactions. In addition, although it is reasonable to expect amorphous minerals in the soil due to natural weathering, the actual content of Al- and Fe-(hydr)oxides of the soil was not measured. Thus, there is no approximation of the quantity of potentially positively charged sites or their availability. Simultaneously, available phosphorous was reported for the soil, which might indicate that positively charged sorption sites could already be saturated. With regards to the agricultural background of the soil, it is likely to expect high amounts of negatively charged phosphate in the soil due to fertilizer applications. On the other hand, particle-specific properties might amplify nanoplastic mobility. The raspberry-shell PS-nanoplastics were coated with sodium dodecyl sulphate, a surfactant stabilizing the dispersion. An increased mobility of nanoparticles by coating due to steric stabilization has been observed by He et al. (2019). Correspondingly, the sodium dodecyl sulphate may enhance transport by preventing interactions between the nanoplastic and soil constituents through electrosteric repulsion. In order to assess the impact of the surfactant on the particle mobility, additional steps for removing the surfactant layer may be considered for further investigations.

In the current model, particle removal from the bulk solution is considered a result of attachment. However, apart from material properties, other fate processes similarly contribute to transport or retention dynamics. Due to the earlier breaking point, nanoplastics appear to be moving faster through the column than the conservative tracer. This indicates that the nanoplastics are subject to size exclusion, so that transport is restricted to larger pores in which higher flow velocities predominate (Bear, 2018). Considering the small size of nanoplastics used in this study (256 nm), unless particles engage in heteroaggregation substantially increasing their size, size exclusion would not be expected to occur. The affinity of the used particles for heteroaggregation has been shown by Mitrano et al. (2019). Thus, it is likely that particles associate with natural colloids present in the soil pore water.

Notably, even though the attachment rate was low, some particles were retained in the soil column, as indicated by an incomplete recovery of nanoplastics in the effluent. Due to challenges with background concentrations of the metal-tracer palladium, the hyper-exponential decrease of retained particles with depth reported in numerous studies on nanoparticle retention in soils (Bradford et al., 2004; Bradford and Leij, 2018; Jiang, 2018) could not be observed. While general trends of the BTC were simulated successfully by applying attachment efficiencies as well as attachment and detachment rate coefficients, some observations could not be captured by

the models. Nanoplastic breakthrough curves of the longer columns displayed fluctuations in effluent concentrations by the development of multiple peaks. One possible explanation is the occurrence of blocking effects, as attachment sites get successively occupied by particles. Another explanation is the occurrence of detachment simultaneously with attachment, which might explain the smaller secondary and tertiary peaks, as well as the tailing observed in the data. However, by including detachment, the multiple peaks could not be adequately simulated by the model, although the fit for one replicate improved. Detachment rates were generally significantly lower than attachment rates. An observation shared with other studies is the variability of transport parameters between replicate columns when using natural soils (Cornelis et al., 2013). Despite homogenization of the soil and applications of the same experimental setup and conditions, natural soils are heterogeneous in their composition and packing might have introduced variations influencing particle transport. In this regard, the basic assumption of a representative particle size in mathematical models may not be able to sufficiently model variations (Riva et al., 2008). Further, differentiation between particle retention as a result of attachment or straining in models is still in development. In the currently applied model, it is not possible to reliably quantify the contribution of straining to nanoplastic retention in the soil columns (Bradford et al., 2004).

The currently applied system assumes a steady-state system with a constant and homogeneous flux of water through the column. However, even under saturated conditions pore water in natural soils does not move at the same flow velocity, with some of the soil pore water being relatively immobile. Riva et al. (2008) found the spatial variability of hydraulic properties to be a determining factor influencing transport of particles. Observed tailing might thereby also be a result of heterogenous flow in the soil pores.

Despite kinetic parameters aiming to describe the general attachment and detachment behaviour of a specific material, the values remain tied to underlying assumptions and specific conditions under which they have been obtained. Conditions prevailing in natural soils are mostly variably-saturated, with soils undergoing periods of wetting, saturation and drying. Although the results obtained in this study will remain relevant for instances of saturation, higher retention of particles in the soil is expected for prevailing field conditions. With increasing desaturation of the soil, the connectivity of water-filled pores and subsequently hydraulic conductivity declines strongly (Hillel, 2003). Previous studies found that colloid retention increased with declining water content, due to restrained transport by increasing fractions of stagnant water, film straining and additional interactions at the air-water interface (Fujita and Kobayashi, 2016; Torkzaban et al., 2008). Thus, the mobility determined in saturated column studies should be regarded as the worst-case scenario, i.e. maximum transport that can be expected for nanoplastics.

Nanoplastic transport in soils by bioturbation

For actual field conditions, soils are more likely unsaturated. Limited mobility of polystyrene nanoplastics under variably-saturated conditions could be observed during our investigations on biologically mediated transport at precipitation intensities of 8.2 mm week^{-1}. While aiming at quantifying the impact of earthworm burrowing on nanoplastic displacement, control plots were subject to water application at the

top of the plots over the course of four weeks. In the absence of earthworms in control plots, nanoplastic transport was restricted to water movement only. Nanoplastics could not be detected in the lower soil profile of control plots indicating that displacement of particles in unsaturated soils by percolating water was at least very limited.

Natural soils are subject to a variety of processes affecting the distribution of pollutants. The quantitatively most dominant processes have to be identified and modelled for a comprehensive exposure and risk assessment. In our study, the presence of anecic earthworms (*Lumbricus terrestris*) caused a significant vertical displacement of nanoplastics away from the top layer with which they were initially added into deeper soil depths. Depending on the prevailing field conditions, it is therefore possible that transport by bioturbation contributes more to the movement of nanoplastics into lower parts of the soil than physical transport by percolating water. Under the influence of bioturbation, a significant increase of nanoplastics in the lower parts of the soil profile was already encountered after one week of exposure, successively increasing with time throughout the duration of the experiment (28 days). Observed trends are comparable to those observed during previous studies on biologically mediated transport of microplastics conducted by Rillig et al. (2017) and Huerta Lwanga et al. (2017). In both cases, transport of polyethylene microplastics by bioturbation was confirmed after relatively short time periods (14 and 21 days).

Notably, both available studies on plastic transport by bioturbation do not further investigate potential time-dependency of bioturbation dynamics, as results are based on sampling at a single timepoint. In the current study, bioturbation intensities were documented in weekly intervals over a total of four weeks capturing temporal trends. Thereby, it was possible to implement a bioturbation model for predicting particle concentrations based on a time-dependent bioturbation rate. The bioturbation rate derived in our experiment was $k_{bioturb} = 5.7 \times 10^{-6}$ s^{-1} (at $d_l = 0.01$). Despite the lower worm density, this bioturbation rate is slightly higher than the values reported by Baccaro et al. (2019) for silver sulphide nanoparticle transport, i.e. $k_{bioturb} = 3.4 \times 10^{-6}$ s^{-1} when adjusted to the same depth step as in the current study. Consequently, it appears that bioturbation and associated transport of particles was more strongly pronounced in the nanoplastic experiment. Reasons for this difference could be related to material properties of the nanoparticles, the selected earthworm species, or differences in the experimental setups. While it is difficult to disentangle the relative contribution of each factor in the current study setup, some potential causes can be pointed out. The higher bioturbation rate contrasts with the clear inverse relationship between size and biologically mediated transport of microplastics established by Rillig et al. (2017). The nanoparticles applied by Baccaro et al. (2019) were much smaller (28 ± 9 nm) than the nanoplastics of the current study (256 ± 4 nm), whereas the microplastics used by Rillig et al. (2017) were much larger (710 µm). It is possible that the enhanced mobility observed by Rillig et al. (2017) decreases below a certain particle size and other factors gain relative importance. Not only species but ecological type differed with the current study using *L. terrestris* (anecic) and *Lumbricus rubellus* (endogeic) being used by Baccaro et al. (2019). Therefore, different bioturbation rates may be related to burrowing and feeding behaviour of the earthworm species used. As *L. terrestris* feeds on litter on

the surface, it is more likely to be in repeated contact with the spiked material than the litter and soil-feeding *L. rubellus* scavenging also below the surface (Fründ et al. 2010). In addition, very high worm densities may have a negative impact on earthworm fitness and activity as a reaction to competition and stress.

Considering the overall fit, the applied model consistently underestimated the transfer of nanoplastics into deeper depths while overestimating mixing into the layer directly adjacent to the spiked top layer. While the magnitude of displaced nanoplastics was still related to soil depth, with decreasing concentrations along the soil profile, the proportions of nanoplastics displaced into the lower profile were larger than simulated ones. Highest deviations were found in the lowest sampling layer (15-29 cm). Correspondingly, fits were improved when down-prioritizing this layer, resulting in $k_{bioturb} = 2.9 \times 10^{-6}$. For particle transport, complete and instantaneous mixing was assumed to occur only for adjacent layers. Thereby, the transport predicted by the model resembles the process of diffusion, favouring a successive vertical distribution of the pollutant. However, actual earthworm activity is not restricted to adjacent layers and it is possible that transport occurs along the entire column. *L. terrestris* is known for its preferred vertical burrows, thereby nanoplastics can be transported directly from the surface to other parts of the soil over larger distances due ingestion, adhesion and preferential flow (Wilkinson et al., 2009). For improving or adjusting the model, the specific mode of transport that predominates the vertical displacement of nanoplastics under the influence of bioturbation is decisive. Although first attempts have been made to explicitly incorporate ingestion and egestion into bioturbation models (Jarvis et al., 2010), there is still a lack of a comprehensive model considering all modes of transport associated with bioturbation, including preferential flow. With regards to the microplastic studies conducted by Huerta Lwanga et al. (2017) it is likely that particles are mixed mechanically or adhere to earthworm surfaces and are thereby incorporated into burrow walls. Additionally, Rillig et al. (2017) were able to detect microplastics in casts of earthworms confirming that particles are also ingested and egested. As water has been added by spraying to keep the soil moisture at optimal levels for earthworm activity, transport by preferential flow through earthworm burrows is also a possible pathway. Since general transport by advection could not be confirmed, it is uncertain how much this pathway contributed in the experiment. More defined sampling schemes may be able to capture finer spatial patterns currently not visible in the applied experimental setup.

Although nanoplastics were detected in the layer directly below the initial spiked layer, these plastics can neither be fully attributed to earthworm burrowing activity for the bioturbation plots, nor to advective-dispersive transport for the control plots. Especially for the boundary between the first and second layer, sampling accuracy is crucial in order to prevent mixing to occur during sampling, artificially enhancing the assumed transported nanoplastic concentration when samples are homogenised. In bioturbation and control plots, it is likely that the sampling setup significantly contributed to detected concentrations as high amounts of nanoplastics in the overlying layer would already be transferred in minimal sampling errors. Consequently, the detected nanoplastics in the second sampling layer can neither be fully attributed to earthworm burrowing activity for the bioturbation plots, nor to advective-dispersive transport for the control plots. Even though it is likely that some transport with

percolating water occurred in the control plots, it is not possible to reliably assess its contribution in the current sampling approach.
The impact of bioturbation on nanoplastic transport holds important implications for exposure estimates in risk assessments. As nanoplastics enter soils with sludge or other pathways on the surface, initial concentrations are highly localized. For soils used for agricultural production, exposure levels of crops to nanoplastics will be dependent on the applied soil management. In conservative soil management, tilling, and to a lower extend ploughing, is likely to accelerate the mixing of nanoplastics with the uppermost 50 cm of the soil and reduce initial exposure levels of plant seedlings before germination. However, even in no-till and direct drilling crop management where disturbance of the soil is minimized, nanoplastic exposure will be reduced over time through the diluting effect of bioturbation as particles are successively displaced into lower soil depths. Consequently, the risk of toxic effects from additives released from the plastics might be reduced as particles are less localized. The relative contribution of bioturbation to this mixing effect varies with the soil management applied. The depth of displacement by earthworm burrowing activity is dependent on their travel distance. *Lumbricus terrestris* is mostly reported to move between the surface and the first 50 cm of the soil, but common depths of 1 m or more are also reported (Fründ et al., 2010). Consequently, even in conservative soil management systems, bioturbation may play an important role in further transport into deeper soil.
Despite the influence of bioturbation shown in this study, according to the applied bioturbation model hypothetical total mixing of the soil would still take 2-3 years under unchanged experimental conditions. Mixing of plastic particles into the soil profile is thus a relatively slow process. Nevertheless, it remains relevant considering the long history of plastic emissions to agricultural soils by sewage sludge application.

Environmental relevance of study and implications for plastic pollution of soils

Results indicate that, under field conditions with variable soil moisture contents, nanoplastic mobility is limited. However, there is considerable potential for successive displacement of plastics by physical and/or biological processes. While bioturbation has been shown to contribute more to the mobility of nanoplastics under variable water contents in soil, percolating water may still cause considerable movement under saturated conditions in the soil. In addition, advective transport of plastics may still be relevant, for example when plastics are added with water such as in irrigation systems in agriculture.
Overall, it is reasonable to expect that whilst nanoplastics entering the soil with soil amendments, runoff or through atmospheric deposition, are firstly accumulated in soils, they are subject to further transport processes. Under long-term influences of the synergetic effect of soil management practices, precipitation and bioturbation, nanoplastics may be increasingly displaced into lower parts of the soil profile. This may reduce exposure levels on the surface, including potential physical and chemical toxicity effects on crops and terrestrial organisms. Additionally, for especially urban soils, this may reduce potential impacts on human health. Conversely, as nanoplastics are transferred into lower depths of the soil, other risks arise. In particular, potential contamination of groundwater with small plastic particles has been

repeatedly raised as a concern. It is necessary to further investigate whether under favourable conditions for transport a significant transfer of small plastics to other environmental compartments, such as freshwater or marine systems, may occur through runoff, percolating water or groundwater flow. Additionally, as historically and recently emitted nanoplastics are successively displaced into deeper soil layers, they may become more persistent as a result of decreasing microbial activity at those depths (Baccaro et al., 2019). Over longer timespans and continuous input into the soil from the surface, there is a risk for substantial accumulation of nanoplastics in the lower parts of the soil.

The obtained kinetic transport parameters apply to specific nanoplastics under specific transport conditions, i.e. completely water filled pores and direct input into the soil, and can be considered a worst-case scenario of plastic mobility. However, the raspberry-shell PS-nanoplastics applied in this study are of one particle size and one specific plastic type only. The terms micro- and nanoplastics comprise a wide array of polymers, and the few studies attempting to quantify plastics in environmental samples have found a wide distribution of particle sizes and types (Andrady, 2017; Kawecki and Nowack, 2019). In addition, the attachment behaviour of nanoparticles has been confirmed to be strongly dependent on particles size (Taghavy et al., 2015). Thus, extrapolation of the obtained kinetic transport parameters to small plastics of other sizes or types is not yet possible and requires additional investigations, including different materials, surface morphologies and chemical compositions. Long-term degradation of plastics in soils may further cause a change in their behaviour and thus, environmental fate. Secondary nanoplastics previously subject to weathering have been found to display changed chemical and physical properties, such as surface charges or roughness (Andrady, 2017). Interactions with the bulk soil or other colloids may differ substantially, thus impact of changed material properties on attachment, detachment, hydrophobic interactions and aggregation require further investigation.

In the current study, particle transport has been studied using only one specific natural soil. Physicochemical conditions of the soil influence nanoparticle and colloid attachment and release (Bradford et al., 2015). Consequently, the extrapolation of obtained transport parameters to other soils is problematic because hydraulic properties of the soil, and the solution chemistry of the soil pore water will affect the observed retention or leaching of particles. Currently, the derived parameters are only valid within the limitations of applied experimental conditions. In our study, variations were already observed for replicate soil columns. In order to obtain meaningful kinetic parameters that are more widely applicable, attachment and detachment of nanoplastics need to be quantified in various soils.

A major pathway of nanoplastics to soils is through sewage sludge application to agricultural fields as fertilizer. Navarro et al. (2014) found that nanomaterials added to soils with sludge decreased their mobility as compared to direct injections. As Mitrano et al. (2019) showed, nanoplastics show a high tendency to engage in heteroaggregation with organic material. Correspondingly, it is reasonable to expect changed mobility under different application modes for advective transport as well as biologically mediated transport. While particles might first have to be remobilized in order for transport with percolating water to occur, for bioturbation the presence of nanoplastics in sludge might even increase vertical transport. Although it is

yet unknown whether mechanical mixing, ingestion and excretion, or preferential flow is the major contributing mechanism of nanoplastic displacement due to bioturbation, the availability of food sources is likely to promote movement of earthworms to the surface. Thus, the results of the bioturbation study may be more widely applicable to other nanoplastic types.

In our bioturbation study, a plastic concentration corresponding to 7.5 kg ha^{-1} was applied. While this is still within the lower range of detected concentrations in industrial sites reported by Fuller and Gautam (2016), it is currently uncertain whether this is applicable to agricultural soils in the context of historical plastic inputs. Most environmental concentrations are expected to be below the concentrations used in this study. It is thus necessary to further investigate bioturbation intensity as a function of plastic concentration, considering different plastic emission scenarios. Moreover, the used earthworm densities exceeded expected field densities in this study (Fründ et al. 2010). Thus, actual displacement by burrowing activity of earthworms in the field might be less pronounced than found here. The dominant role of earthworms in biologically mediated displacement of particles is well documented (Meysman et al., 2006; Taylor et al., 2018; Wilkinson et al., 2009). However, while transport by bioturbation was based on the burrowing activity of a single species, the deep-burrowing *L. terrestris*, the presence of different important bioturbating species may result in cumulative effects enhancing the mobility of nanoplastics in natural soils.

For soil management, the spread of nanoplastics is yet of unknown consequences. Investigations on the potential exposure of terrestrial organisms, crops and human health through soils need to be supplemented by hazard assessments that address potential physical and chemical toxicity of nanoplastics. In this study, the presence of plastics in the soil did not have detectable significantly negative impacts on earthworm development as opposed to results from exposure studies of earthworms to plastics reported by Huerta Lwanga et al. (2016). However, conditions in this study aimed at promoting maximum bioturbation activity considering temperatures and humidity. It is not possible to rule out potential long-term impacts on individuals or the community. Earthworms in different developmental stages, i.e. during growing phases, may be more susceptible to physical or chemical toxicity of plastics. In addition, the PS-nanoplastics did not comprise any additives, such as flame retardants or plasticizers. For comprehensive risk assessments, the uptake of nanoplastics by terrestrial organisms and plants needs further research on the chemical and physical toxicity effects and potential trophic transfers in order to reliably estimate hazards.

6 Conclusion

The mobility of palladium-doped raspberry-shell polystyrene nanoplastics of 256 nm size was investigated and quantitative fate descriptors obtained through process-studies on advection-driven and biologically mediated transport. Nanoplastics were highly mobile in saturated systems under the influence of advection. Leaching tests revealed little retention of nanoplastics in natural soils. Inverse modelling in HYDRUS-1D was successfully applied to derive kinetic transport parameters (α_{att}, k_{att}, k_{det}) from breakthrough curves of eluted nanoplastic concentrations. Attachment efficiencies of the PS-nanoplastics were low. There were further indications for detachment, but observed trends could not be adequately captured by the applied models. Conversely, a very limited mobility of nanoplastics was observed under unsaturated and thus more representative field conditions. Transport of nanoplastics with percolating water from recurring water applications could not be detected in the control plots of the bioturbation studies. While this indicates that soils may indeed act as sinks for micro- and nanoplastics, the spatial distribution and mobility of particles in natural soils will be further modified by the activity of soil biota. Earthworm bioturbation caused a significant displacement of nanoplastics into lower soil layers. Bioturbation rates ($k_{bioturb}$) describing the observed bioturbation intensity were calculated by applying a bioturbation model. While providing good predictions when fit to separate layers, the bioturbation model was not able to adequately simulate the observed concentrations in all layers simultaneously. In particular, the model underestimated the encountered nanoplastic concentrations in the deeper soil profile. Adjustments of the model are needed in order to accurately describe the impact of earthworm bioturbation on the vertical displacement of nanoplastics. Even though bioturbation was found to be a relatively slow process, in the context of the long history of sewage sludge application and associated historic and recent plastic emissions, its contribution to the final distribution of micro- and nanoplastics in soils may be more important than transport by percolation. While the results of this study provide a first insight into the importance of different transport processes for plastics in a natural soil, it is not yet possible to extrapolate results to other sizes and types of nanoplastics. In order to increase the environmental relevance of findings, plastics of different chemical composition and physical structure should be included in further studies using a wider variety of soils.

References

86/278/EEC, 1986. Council Directive 86/278/EEC of 12 June 1986 on the protection of the environment, and in particular of the soil, when sewage sludge is used in agriculture. Available at: https://eur-lex.europa.eu/legal-content/EN/TXT/PDF/?uri=CELEX:31986L0278&from=EN [Accessed: 2019-08-02].

Andrady, A.L., 2017. The plastic in microplastics: A review. *Marine Pollution Bulletin 119 (1)*, 12-22. DOI: 10.1016/j.marpolbul.2017.01.082.

Auta, H.S., Emenike, C.U., Fauziah, S.H., 2017. Distribution and importance of microplastics in the marine environment: A review of the sources, fate, effects, and potential solutions. *Environment International 102*, 165-176. DOI: 10.1016/j.envint.2017.02.013.

Avio, C.G., Gorbi, S., Regoli, F., 2017. Plastics and microplastics in the oceans: From emerging pollutants to emerged threat. *Marine Environmental Research 128*, 2-11. DOI: 10.1016/j.marenvres.2016.05.012.

Baalousha, M., Cornelis, G., Kuhlbusch, T.A.J., Lynch, I., Nickel, C., Peijnenburg, W., van den Brink, N., 2016. Modeling Nanomaterial Fate and Uptake in the Environment: Current Knowledge and Future Trends. *Environmental Science: Nano 3 (2)*, 1-38. DOI: 10.1039/C5EN00207A.

Baccaro, M., Harrison, S., Berg, H. van den, Sloot, L., Hermans, D., Cornelis, G., Gestel, C.A.M. van, Brink, N.W. van den, 2019. Bioturbation of Ag_2S-NPs in soil columns by earthworms. *Environmental Pollution 252*, 155-162. DOI: 10.1016/j.envpol.2019.05.106.

Bardgett, R.D., 2005. The biology of soil: a community and ecosystem approach. Oxford University Press, New York, 256 p.

Bear, J., 2018. Modeling Phenomena of Flow and Transport in Porous Media, Theory and Applications of Transport in Porous Media. Springer Nature. 742 p. DOI: 10.1007/978-3-319-72826-1.

Beauchemin, D., 2017. Inductively Coupled Plasma Mass Spectrometry Methods. In: Lindon, J.C., Tranter, G.E., Koppenaal, D.W. (Eds.*), Encyclopedia of Spectroscopy and Spectrometry*. Academic Press, Oxford, pp. 236–245. DOI: 10.1016/B978-0-12-409547-2.11222-3.

Bergmann, M., Mützel, S., Primpke, S., Tekman, M.B., Trachsel, J., Gerdts, G., 2019. White and wonderful? Microplastics prevail in snow from the Alps to the Arctic. *Science Advances 5*. DOI: 10.1126/sciadv.aax1157.

Bhattacharjee, S., 2016. DLS and zeta potential - What they are and what they are not? *Journal of Controlled Release 235*, 337-351. DOI: 10.1016/j.jconrel.2016.06.017.

Bläsing, M., Amelung, W., 2018. Plastics in soil: Analytical methods and possible sources. *Science of the Total Environment 612*, 422-435. DOI: 10.1016/j.scitotenv.2017.08.086.

Blume, H.-P., Brümmer, G.W., Fleige, H., Horn, R., Kandeler, E., Kögel-Knabner, I., Kretzschmar, R., Stahr, K., Wilke, B.-M., 2016. Scheffer/Schachtschabel. Soil Science. Springer Berlin Heidelberg, 630 p. DOI: 10.1007/978-3-642-30942-7.

Bouché, M.B., 1977. Strategies lombriciennes 25. *Ecologial Bulletins 25*. 122-132. Available at: https://www.jstor.org/stable/20112572.

Bradford, S.A., Bettahar, M., Šimůnek, J., van Genuchten, M.Th., 2004. Straining and Attachment of Colloids in Physically Heterogeneous Porous Media. *Vadose Zone Journal 3 (2)*, 384-394. DOI: 10.2113/3.2.384.

Bradford, S.A., Leij, F.J., 2018. Modeling the transport and retention of polydispersed colloidal suspensions in porous media. *Chemical Engineering Science 192*, 972-980. DOI: 10.1016/j.ces.2018.08.037.

Bradford, S.A., Šimůnek, J., Bettahar, M., Van Genuchten, M.Th., Yates, S.R., 2003. Modeling Colloid Attachment, Straining, and Exclusion in Saturated Porous Media. *Environmental Science & Technology 37*, 2242–2250. DOI: 10.1021/es025899u.

Bradford, S.A., Torkzaban, S., Walker, S.L., 2007. Coupling of physical and chemical mechanisms of colloid straining in saturated porous media. *Water Research 41 (13)*, 3012-3024. DOI: 10.1016/j.watres.2007.03.030.

Brenner, I.J., 2017. Inductively Coupled Plasma Mass Spectrometry Applications. In: Lindon, J.C., Tranter, G.E., Koppenaal, D.W. (Eds.), *Encyclopedia of Spectroscopy and Spectrometry*. Academic Press, Oxford, pp. 229-235. Available at: http://www.sciencedirect.com/science/article/pii/B9780128032244000571.

Brusseau, M.L., 2019. Chapter 7 - Physical Processes Affecting Contaminant Transport and Fate In: Brusseau, Mark L., Pepper, I.L., Gerba, C.P. (Eds.), *Environmental and Pollution Science (Third Edition)*. Academic Press, pp. 103–112. Available at: http://www.sciencedirect.com/science/article/pii/B9780128147191000070.

Chapin, F.S III., Matson, P.A., Mooney, H., 2002. Principles of Terrestrial Ecosystem Eology. Second Edition. Springer Berlin, Heidelberg. 447 p. DOI: 10.1007/978-1-4419-9504-9.

Chinju, H., Kuno, Y., Nagasaki, S., Tanaka, S., 2001. Deposition Behavior of Polystyrene Latex Particles on Solid Surfaces during Migration through an Artificial Fracture in a Granite Rock Sample. *Journal of Nuclear Science and Technology 38 (6)*, 439-443. DOI: 10.1080/18811248.2001.9715051.

Cicchella, D., Vivo, B.D., Lima, A., 2003. Palladium and platinum concentration in soils from the Napoli metropolitan area, Italy: possible effects of catalytic exhausts. *Science of the Total Environment 308 (1-3)*, 121-131. DOI: 10.1016/S0048-9697(02)00632-0.

Cornelis, G., 2015. Fate descriptors for engineered nanoparticles: the good, the bad, and the ugly. *Environmental Science: Nano 2*, 19-26. DOI: 10.1039/c4en00122b.

Cornelis, G., Adams, J., Green-Etxabe, A., Lofts, S., Lahive, E., Norrfors, K., Seijo, M., Stoll, S., Nickel, C., van Gestel, K., 2018. Soil property – NM fate relationships. (Nanofase Deliverable D7.2), Horizon 2020 project Nanofase.

Cornelis, G., Hund-Rinke, K., Kuhlbusch, T., van den Brink, N., Nickel, C., 2014. Fate and Bioavailability of Engineered Nanoparticles in Soils: A Review. *Critical Reviews in Environmental Science and Technology 44 (24)*, 2720-2764. DOI: 10.1080/10643389.2013.829767.

Cornelis, G., Pang, L., Doolette, C., Kirby, J.K., McLaughlin, M.J., 2013. Transport of silver nanoparticles in saturated columns of natural soils. *Science of the Total Environment 463-464*, 120-130. DOI: 10.1016/j.scitotenv.2013.05.089.

da Costa, J.P., Santos, P.S.M., Duarte, A.C., Rocha-Santos, T., 2016. (Nano)plastics in the environment – Sources, fates and effects. *Science of the Total Environment 566-567*, 15-26. DOI: 10.1016/j.scitotenv.2016.05.041.

Destandau, E., Michel, T., Elfakir, C., 2013. Microwave-Assisted Extraction, in: RSC Green Chemistry, 113–156. DOI: 10.1039/9781849737579-00113.

EC, 2011. Commission recommendation of 18 October 2011 on the definition of nanomaterial (Text with EEA relevance) (2011/696/EU), Official Journal of the European Union. Available at: https://eur-lex.europa.eu/legal-content/EN/TXT/PDF/?uri=OJ:L:2011:275:FULL&from=EN [Accessed: 2019-07-20].

Elimelech, M., Gregory, J., Jia, X., Williams, R.A., 1995. Particle Deposition & Aggregation. Measurement, Modelling and Simulation. Butterworth Heinemann, Woburn, USA. First Edition. 458 p.

Essington, M., 2004. Soil and water chemistry: an integrative approach. Second edition. CrC Press. 656 p.

Fründ, H.-C., Butt, K., Capowiez, Y., Eisenhauer, N., Emmerling, C., Ernst, G., Potthoff, M., Schädler, M., Schrader, S., 2010. Using earthworms as model organisms in the laboratory: Recommendations for experimental implementations. *Pedobiologia 53*, 119-125. DOI: 10.1016/j.pedobi.2009.07.002.

Fujita, Y., Kobayashi, M., 2016. Transport of colloidal silica in unsaturated sand: Effect of charging properties of sand and silica particles. *Chemosphere 154*, 179-186. DOI: 10.1016/j.chemosphere.2016.03.105.

GESAMP, 2016. Sources, fate and effects of microplastics in the marine environment: Part 2 of a global assessment. *Reports and Studies GESAMP 93*, 220 p. Available

at: http://www.gesamp.org/publications/microplastics-in-the-marine-environment-part-2 [Accessed: 2019-07-04].

GESAMP, 2015. Sources, fate and effects of microplastics in the marine environment: *A global assessment. Reports and Studies GESAMP 90*, 96 p. Available at: https://ec.europa.eu/environment/marine/good-environmental-status/descriptor-10/pdf/GESAMP_microplastics%20full%20study.pdf [Accessed: 2019-07-04].

Gewert, B., Ogonowski, M., Barth, A., MacLeod, M., 2017. Abundance and composition of near surface microplastics and plastic debris in the Stockholm Archipelago, Baltic Sea. *Marine Pollution Bulletin 120*, 292-302. DOI: 10.1016/j.marpolbul.2017.04.062.

Gustafsson, J.P. 2013. Visual MINTEQ version 3.1.

He, J., Wang, D., Zhou, D., 2019. Transport and retention of silver nanoparticles in soil: Effects of input concentration, particle size and surface coating. *Science of the Total Environment 648*, 102-108. DOI: 10.1016/j.scitotenv.2018.08.136.

Hillel, D. (Ed.), 2003. Introduction to Environmental Soil Physics. Academic Press, Burlington, First Edition. 494 p.

Horton, A.A., Walton, A., Spurgeon, D.J., Lahive, E., Svendsen, C., 2017. Microplastics in freshwater and terrestrial environments: Evaluating the current understanding to identify the knowledge gaps and future research priorities. *Science of the Total Environment 586*, 127–141. DOI: 10.1016/j.scitotenv.2017.01.190.

Huerta Lwanga, E., Gertsen, H., Gooren, H., Peters, P., Salánki, T., Ploeg, M. van der, Besseling, E., Koelmans, A.A., Geissen, V., 2017. Incorporation of microplastics from litter into burrows of Lumbricus terrestris. *Environmental Pollution 220*, 523-531. DOI: 10.1016/j.envpol.2016.09.096.

Huerta Lwanga, E., Gertsen, H., Gooren, H., Peters, P., Salánki, T., van der Ploeg, M., Besseling, E., Koelmans, A.A., Geissen, V., 2016. Microplastics in the Terrestrial Ecosystem: Implications for Lumbricus terrestris (Oligochaeta, Lumbricidae). *Environmental Science & Technology 50*, 2685–2691. DOI: 10.1021/acs.est.5b05478.

ISO 11466:1995, 1995. ISO 11466:1995. Soil quality -- Extraction of trace elements soluble in aqua regia. ISO, Geneva.

Jarvis, N.J., Taylor, A., Larsbo, M., Etana, A., Rosén, K., 2010. Modelling the effects of bioturbation on the re-distribution of 137Cs in an undisturbed grassland soil. *European Journal of Soil Science 61 (1)*, 24-34. DOI: 10.1111/j.1365-2389.2009.01209.x.

Jiang, J.-Q., 2018. Occurrence of microplastics and its pollution in the environment: A review. *Sustainable Production and Consumption 13*, 16-23. DOI: 10.1016/j.spc.2017.11.003.

Jiang, X., Tong, M., Lu, R., Kim, H., 2012. Transport and deposition of ZnO nanoparticles in saturated porous media. *Colloids and Surfaces A: Physicochemical and Engineering Aspects 401*, 29-37. DOI: 10.1016/j.colsurfa.2012.03.004.

Kawecki, D., Nowack, B., 2019. Polymer-specific modeling of the environmental emissions of seven commodity plastics as macro- and microplastics. *Environmental Science & Technology 53 (16)*, 9664-9676. DOI: 10.1021/acs.est.9b02900.

Kuznar, Z.A., Elimelech, M., 2007. Direct microscopic observation of particle deposition in porous media: Role of the secondary energy minimum. *Colloids and Surfaces A: Physicochemical and Engineering Aspects 294 (1-3)*, 156-162. DOI: 10.1016/j.colsurfa.2006.08.007.

Lazouskaya, V., Jin, Y., 2008. Colloid retention at air-water interface in a capillary channel. *Colloids and Surfaces A: Physicochemical and Engineering Aspects 325 (3)*, 141-151. DOI: 10.1016/j.colsurfa.2008.04.053.

Lebreton, L., Andrady, A., 2019. Future scenarios of global plastic waste generation and disposal. *Palgrave Communications 5 (1)*, 6. DOI: 10.1057/s41599-018-0212-7.

Lee, H., Shim, W.J., Kwon, J.-H., 2014. Sorption capacity of plastic debris for hydrophobic organic chemicals. *Science of the Total Environment 470–471*, 1545-1552. DOI: 10.1016/j.scitotenv.2013.08.023.

Li, M., Greenfield, B.K., Nunes, L.M., Dang, F., Liu, H., Zhou, D., Yin, B., 2019. High retention of silver sulfide nanoparticles in natural soils. *Journal of Hazardous Materials 378*, 120735. DOI: 10.1016/j.jhazmat.2019.06.012.

Liang, Y., Hilal, N., Langston, P., Starov, V., 2007. Interaction forces between colloidal particles in liquid: Theory and experiment. *Advances in Colloid and Interface Science 134-135*, 151-166. DOI: 10.1016/j.cis.2007.04.003.

LTU, 2014. Materialåtervinning av uttjänta däck. Available at: https://www.ltu.se/research/subjects/Geotechnical-engineering/Dackatervinningsportalen/Materialatervinning [Accessed: 2019-06-20].

Magnusson, K., Eliasson, K., Fråne, A., Haikonen, K., Hultén, J., Olshammer, M., Stadmark, J., Voisin, A., IVL Svenska Miljöinstitutet, 2017. Swedish sources and pathways for microplastics to the marine environment. A review of existing data. *IVL Swedish Environmental Research Institute 2016 Reports C 183*.

Malvern Instruments Ltd., 2009. Zetasizer Nano User Manual. MAN0317 Issue 5.0. Worcestershire. Available at: http://www.biophysics.bioc.cam.ac.uk/wp-content/uploads/2011/02/zetasizer_nanozs_manual.pdf [Accessed: 2019-05-10].

Meysman, F.J.R., Middelburg, J.J., Heip, C.H.R., 2006. Bioturbation: a fresh look at Darwin's last idea. *Trends in Ecology & Evolution 21 (12)*, 688-695. DOI: 10.1016/j.tree.2006.08.002.

Milieu Ltd, WRc, RPA, 2010. Environmental, economic and social impacts of the use of sewage sludge on land. Final report. Part I: Overview Report. Available at: http://ec.europa.eu/environment/archives/waste/sludge/pdf/part_i_report.pdf [Accessed: 2019-06-20].

Ministry of Environment, 2018. Inquiry to propose ban on spreading sewage sludge on farmland and a phosphorus recycling requirement. *Government Offices of Sweden.*

Press release. Available at: https://www.government.se/press-releases/2018/07/inquiry-to-propose-ban-on-spreading-sewage-sludge-on-farmland-and-a-phosphorus-recycling-requirement/ [Accessed: 2019-06-20].

Mitrano, D.M., Beltzung, A., Frehland, S., Schmiedgruber, M., Cingolani, A., Schmidt, F., 2019. Synthesis of metal-doped nanoplastics and their utility to investigate fate and behaviour in complex environmental systems. *Nature Nanotechnology*, 9. DOI: 10.1038/s41565-018-0360-3.

Muralikrishna, I.V., Manickam, V., 2017. Chapter Eight - Environmental Risk Assessment. In: Muralikrishna, I.V., Manickam, V. (Eds.), Environmental Management. Butterworth-Heinemann, pp. 135-152. DOI: 10.1016/B978-0-12-811989-1.00008-7.

Ng, E.-L., Huerta Lwanga, E., Eldridge, S.M., Johnston, P., Hu, H.-W., Geissen, V., Chen, D., 2018. An overview of microplastic and nanoplastic pollution in agroecosystems. *Science of the Total Environment 627*, 1377-1388. DOI: 10.1016/j.scitotenv.2018.01.341.

Nizzetto, L., Futter, M., Langaas, S., 2016. Are Agricultural Soils Dumps for Microplastics of Urban Origin? *Environmental Science & Technology 50 (20)*, 10777-10779. DOI: 10.1021/acs.est.6b04140.

OECD, 2004. Test No. 312: Leaching in Soil Columns, OECD Guidelines for the Testing of Chemicals, Section 3. OECD Publishing, Paris. Available at: http://www.oecd.org/chemicalsafety/risk-assessment/1948325.pdf [Accessed: 2019-05-12].

Oehlmann, J., Schulte-Oehlmann, U., Kloas, W., Jagnytsch, O., Lutz, I., Kusk, K.O., Wollenberger, L., Santos, E.M., Paull, G.C., Van Look, K.J.W., Tyler, C.R., 2009. A critical analysis of the biological impacts of plasticizers on wildlife. *Philosophical transactions of the Royal Society of London. Series B, Biological sciences 364*, 2047-2062. DOI: 10.1098/rstb.2008.0242.

Phenrat, T., Saleh, N., Sirk, K., Kim, H.-J., Tilton, R., Lowry, G., 2008. Stabilization of aqueous nanoscale zerovalent iron dispersions by anionic polyelectrolytes: Adsorbed anionic polyelectrolyte layer properties and their effect on aggregation and sedimentation. *Journal of Nanoparticle Research 10*, 795-814. DOI: 10.1007/s11051-007-9315-6.

Praetorius, A., Tufenkji, N., Goss, K.-U., Scheringer, M., von der Kammer, F., Elimelech, M., 2014. The road to nowhere: equilibrium partition coefficients for nanoparticles. *Environmental Science: Nano 4*, 317-323. DOI: 10.1039/c4en00043a.

Rahmatpour, S., Mosaddeghi, M.R., Shirvani, M., Šimůnek, J., 2018. Transport of silver nanoparticles in intact columns of calcareous soils: The role of flow conditions and soil texture. *Geoderma 322*, 89-100. https://doi.org/10.1016/j.geoderma.2018.02.016.

Ramos, A.P., 2017. 4 - Dynamic Light Scattering Applied to Nanoparticle Characterization. In: Róz, A.L.D., Ferreira, M., Leite, F. de L., Oliveira, O.N. (Eds.),

Nanocharacterization Techniques, Micro and Nano Technologies. William Andrew Publishing, pp. 99-110. DOI: 10.1016/B978-0-323-49778-7.00004-7.

Raychoudhury, T., Naja, G., Ghoshal, S., 2010. Assessment of transport of two polyelectrolyte-stabilized zero-valent iron nanoparticles in porous media. *Manufactured Nanomaterials in Subsurface Systems 118 (3)*, 143–151. DOI: 10.1016/j.jconhyd.2010.09.005.

Rillig, M.C., Ziersch, L., Hempel, S., 2017. Microplastic transport in soil by earthworms. *Scientific Reports 7 (1362)*, 1-6. DOI: 10.1038/s41598-017-01594-7.

Riva, M., Guadagnini, A., Fernandez-Garcia, D., Sanchez-Vila, X., Ptak, T., 2008. Relative importance of geostatistical and transport models in describing heavily tailed breakthrough curves at the Lauswiesen site. *Journal of Contaminant Hydrology 101 (1)*, 1-13. DOI: 10.1016/j.jconhyd.2008.07.004.

Rodriguez, M.D., 2006. The bioturbation transport of chemicals in surface soils. Louisiana State University.

Schaap, M.G., J. Leij, F., Van Genuchten, M., 2001. ROSETTA: A computer program for estimating soil hydraulic parameters with hierarchical pedotransfer functions. *Journal of Hydrology 251*, 163-176. DOI: 10.1016/S0022-1694(01)00466-8.

Scheirs, J., Priddy, D.B., 2003. Modern Styrenic Polymers: Polystyrenes and Styrenic Copolymers. John Wiley & Sons, Ltd. 757 p. DOI: 10.1002/0470867213.ch17.

Shen, C., Huang, Y., Li, B., Jin, Y., 2010. Predicting attachment efficiency of colloid deposition under unfavorable attachment conditions. *Water Resources Research 46 (11)*, 1-12. DOI: 10.1029/2010WR009218.

Shen, C., Lazouskaya, V., Jin, Y., Li, B., Ma, Z., Zheng, W., Huang, Y., 2012. Coupled factors influencing detachment of nano- and micro-sized particles from primary minima. *Journal of Contaminant Hydrology 134-135*, 1-11. DOI: 10.1016/j.jconhyd.2012.04.003.

Šimůnek, J., Maximilian Köhne, J., Kodešová, R., Šejna, M., 2008. Simulating Nonequilibrium Movement of Water Solutes and Particles Using HYDRUS – A Review of Recent Applications. *Soil Water Research 3*, 42-51. DOI: 10.17221/1200-SWR.

Šimůnek, J., Šejna, M., Saito, H., Sakai, M., Van Genuchten, M.Th., 2009. The HYDRUS-1D Software Package for Simulating the One-Dimensional Movement of Water, Heat, and Multiple Solutes in Variably-Saturated Media. Version 4.08. 332 p. Department of Environmental Sciences, University of California Riverside.

Singh, P., Sharma, V.P., 2016. Integrated Plastic Waste Management: Environmental and Improved Health Approaches. *Procedia Environmental Sciences 35*, 692-700. DOI: 10.1016/j.proenv.2016.07.068.

Solovitch, N., Labille, J., Rose, J., Chaurand, P., Borschneck, D., Wiesner, M.R., Bottero, J.-Y., 2010. Concurrent Aggregation and Deposition of TiO2 Nanoparticles in a Sandy Porous Media. *Environmental Science & Technology 44 (13)*, 4897-4902. DOI: 10.1021/es1000819.

Taghavy, A., Pennell, K.D., Abriola, L.M., 2015. Modeling coupled nanoparticle aggregation and transport in porous media: A Lagrangian approach. *Journal of Contaminant Hydrology 172*, 48–60. DOI: 10.1016/j.jconhyd.2014.10.012.

Taylor, A.R., Lenoir, L., Vegerfors, B., Persson, T., 2018. Ant and Earthworm Bioturbation in Cold-Temperate Ecosystems. *Ecosystems*. DOI: 10.1007/s10021-018-0317-2.

Torkzaban, S., Bradford, S.A., van Genuchten, M.Th., Walker, S.L., 2008. Colloid transport in unsaturated porous media: The role of water content and ionic strength on particle straining. *Journal of Contaminant Hydrology 96 (1)*, 113-127. DOI: 10.1016/j.jconhyd.2007.10.006.

Torrent, L., Marguí, E., Queralt, I., Hidalgo, M., Iglesias, M., 2019. Interaction of silver nanoparticles with mediterranean agricultural soils: Lab-controlled adsorption and desorption studies. *Journal of Environmental Sciences 83*, 205-216. DOI: 10.1016/j.jes.2019.03.018.

Tufenkji, N., Elimelech, M., 2005. Breakdown of Colloid Filtration Theory: Role of the Secondary Energy Minimum and Surface Charge Heterogeneities. *Langmuir 21 (3)*, 841-852. DOI: 10.1021/la048102g.

Tufenkji, N., Miller, G.F., Ryan, J.N., Harvey, R.W., Elimelech, M., 2004. Transport of Cryptosporidium Oocysts in Porous Media: Role of Straining and Physicochemical Filtration. *Environmental Science & Technology 38 (22)*, 5932–5938. DOI: 10.1021/es049789u.

U.S. EPA, 2007. Method 3051A (SW-846): Microwave Assisted Acid Digestion of Sediments, Sludges, and Oils. 30 p. Available at: https://www.epa.gov/sites/production/files/2015-12/documents/3051a.pdf [Accessed: 2019-05-12].

Van Cauwenberghe, L.V., Claessens, M., Vandegehuchte, M.B., Janssen, C.R., 2015. Microplastics are taken up by mussels (Mytilus edulis) and lugworms (Arenicola marina) living in natural habitats. *Environmental Pollution 199*, 10-17. DOI: 10.1016/j.envpol.2015.01.008.

van Middlesworth, J.M., Wood, S.A., 1999. The stability of palladium(II) hydroxide and hydroxy–chloride complexes: an experimental solubility study at 25–85°C and 1 bar. *Geochimica et Cosmochimica Acta 63 (11)*, 1751-1765. DOI: 10.1016/S0016-7037(99)00058-7.

von Moos, N., Burkhardt-Holm, P., Köhler, A., 2012. Uptake and Effects of Microplastics on Cells and Tissue of the Blue Mussel Mytilus edulis L. after an Experimental Exposure. *Environmental Science & Technology 46 (20)*, 11327-11335. DOI: 10.1021/es302332w.

Wichmann, H., A.K. Anquandah, G., Schmidt, C., Zachmann, D., Bahadir, M., 2008. Increase of platinum group element concentrations in soils and airborne dust in an urban area in Germany. *The Science of the Total Environment 388*, 121-127. DOI: 10.1016/j.scitotenv.2007.07.064.

Wiesmeier, M., Spörlein, P., Geuß, U., Hangen, E., Haug, S., Reischl, A., Schilling, B., von Lützow, M., Kögel-Knabner, I., 2012. Soil organic carbon stocks in southeast

Germany (Bavaria) as affected by land use, soil type and sampling depth. *Global Change Biology 18 (7)*, 2233-2245. DOI: 10.1111/j.1365-2486.2012.02699.x.

Wilkinson, M.T., Richards, P.J., Humphreys, G.S., 2009. Breaking ground: Pedological, geological, and ecological implications of soil bioturbation. *Earth-Science Reviews 97 (1)*, 257-272. DOI: 10.1016/j.earscirev.2009.09.005.

Xu, R., Qafoku, N.P., Ranst, E.V., Li, J., Jiang, J., 2016. Chapter One - Adsorption Properties of Subtropical and Tropical Variable Charge Soils: Implications from Climate Change and Biochar Amendment, in: Sparks, D.L. (Ed.), Advances in Agronomy, *Advances in Agronomy 135*. Academic Press, pp. 1-58. DOI: 10.1016/bs.agron.2015.09.001.

Xu, S., Gao, B., Saiers, J.E., 2006. Straining of colloidal particles in saturated porous media. *Water Resources Research 42 (12)*, 10. DOI: 10.1029/2006WR004948.

Xu, S., Qi, J., Chen, X., Lazouskaya, V., Zhuang, J., Jin, Y., 2016. Coupled effect of extended DLVO and capillary interactions on the retention and transport of colloids through unsaturated porous media. *Science of the Total Environment 573*, 564-572. DOI: 10.1016/j.scitotenv.2016.08.112.

Yao, K.-M., Habibian, M.T., O'Melia, C.R., 1971. Water and waste water filtration. Concepts and applications. *Environmental Science & Technology 5 (11)*, 1105-1112. DOI: 10.1021/es60058a005.

Zsolnay, Á., 2003. Dissolved organic matter: artefacts, definitions, and functions. *Ecological aspects of dissolved organic matter in soils 113 (3)*, 187-209. DOI: 10.1016/S0016-7061(02)00361-0.

Acknowledgements

I would like to thank my main supervisor at SLU, Geert Cornelis, and my co-supervisor Bjarne W. Strobel, for giving me this opportunity and their constant support throughout the thesis. A special thanks to collaborators involved in this project, Denise Mitrano, Elma Lahive and Marta Baccaro. In addition, a special thanks to Karin Norrfors for her support in the modelling part of the column transport studies, and my student opponent Isabelle Gough, Karl Dyrhage and all others for their insightful peer review.

Appendix

Table S1: Point of zero charge (pH_{PZC}) for a selection of Aluminum- and Iron-(hydr)oxides common in soils of temperate climates, according to data collected by Essington (2004).

Mineral		pH_{PZC}
Goethite	[α-FeOOH]	9.0
Hematite	[α-Fe_2O_3]	8.5
Gibbsite	[$Al(OH)_3$]	8.9
Kaolinite	[$Al_2Si_2O_5(OH)_4$]	4.7

Table S2: Measurement conditions and quality criteria for the DLS-based size measurements of nanoplastics.

Measurement conditions			Quality criteria		
Replicates	*(nbr)*	3	Signal-to-noise ratio	*(-)*	> 0.9
Readings	*(nbr)*	13	Count rates	*(kcps)*	> 600
Temperature	*(°C)*	18	Attenuator values	*(nbr)*	6-7
Equilibration time	*(s)*	120			
Viscosity of dilution medium	*(cp)*	10.563			

Table S3. Conditions and results of DLS-based size measurements of nanoplastics in serial dilution steps via DLS.

Particle C (mg/l)	Z-average diameter (nm)	PDI	attenuator value	signal-to-noise ratio	derived count rate (kcps)
170	255 ± 2	0.12	6	0.93	64000
85	254 ± 6	0.10	6	0.94	45000
34	258 ± 2	0.10	7	0.93	19000
17	258 ± 3	0.10	7	0.94	14000

Table S4: Z-average diameter measured in ultrapure water in time-series for confirming stable size over a total period of 5 weeks.

Time-series	0 d	1 d	6 d	15 d	5 w
Z-average diameter (nm)	255 ± 2	257 ± 2	255 ± 5	251 ± 6	251 ± 4

Table S5. Results of species distribution simulated using Visual MINTEQ at estimated Pd^{2+} concentrations of 50 µg/l as maximum expected concentrations. Different dilution media were used to test the dependence on chloride concentration.

dilution medium	% of total concentration		saturation index
2.78 % HCl	92.3	$[PdCl_4]^{2-}$	-
	7.0	$[PdCl_3]^-$	-
	0.7	$[PdCl_2]$	-
	0.0	Pd(OH)2(s)	-1.5
ultrapure water	0.4	$[Pd^{2+}]$	-
	99.6	$[PdOH^+]$	-
	0.0	$Pd(OH)_{2(s)}$	5.4

Table S6. Composition of artificial rainwater (according to protocol developed by Cornelis & Norrfors, n. published).

Component		Concentration (M)
Sodium chloride	NaCl	$1.0 \cdot 10^{-5}$
Sodium nitrate	$(NH_4)_2SO_4$	$5.3 \cdot 10^{-6}$
Ammonium sulphate	$NaNO_3$	$5.9 \cdot 10^{-6}$
Calcium chloride	$CaCl_2$	$3.9 \cdot 10^{-6}$

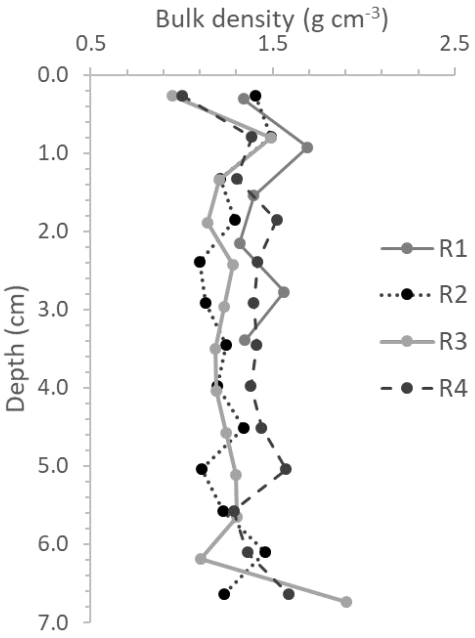

Figure S1: Bulk density (g cm^{-3}) of the replicate columns (R1-R4) from column leaching tests as a function of depth (cm). Measurements were based on the dry soil mass of each segment (approximately 0.5 cm thick) and corresponding volume. Note that the depth increases with distance from the inlet of the column.

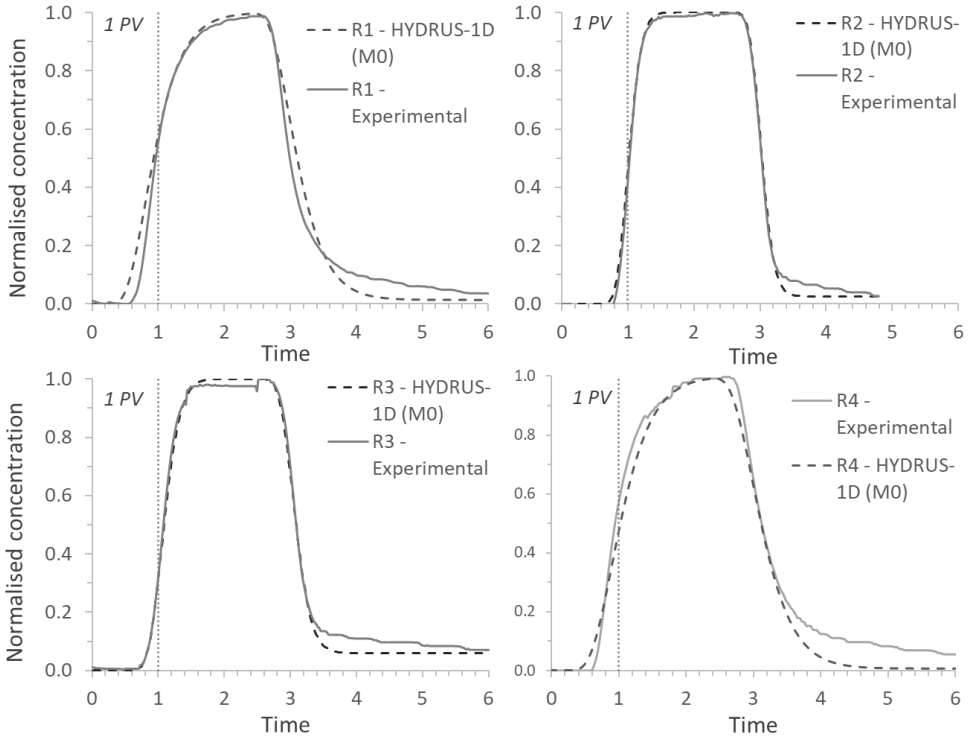

Figure S2: Breakthrough curves of the tracer column experiment, with detected normalised concentrations displayed as a function of time, including experimental and modelled data (M0) using inverse modelling in HYDRUS-1D for all replicate columns (R1-R4).

Table S7: Fit of HYDRUS-1D derived models, expressed as R^2 of the regression of simulated versus observed data, for replicate column 1-4 (R1-R4). Simulations were conducted in HYDRUS-1D. M0: Modelled tracer breakthrough curve, M1: Modelled nanoplastic breakthrough curve considering only attachment, M2: Modelled nanoplastic breakthrough curve based on attachment and detachment. Highest fits were marked in bold.

	R1	R2	R3	R4
M0	0.98449	0.99754	0.99793	0.99114
M1: k_{att}	0.99025	**0.96949**	0.97764	**0.96070**
M1: α_{att}	**0.99026**	**0.96949**	0.99244	0.96036
M2: k_{att}	0.98947	0.96936	**0.99326**	0.95945
M2: α_{att}	0.99025	0.96934	0.99325	0.95947

Table S8: Summary of mean earthworm length and weight before and after experiment for each triplicate set after 1-4 weeks in bioturbation plots (T1-T4).

	fresh weight earthworms (g)		mean length earthworms (cm)	
	initial	final	initial	final
T1	6.0 ± 0.9	5.3 ± 1.0	15.3	16.1
T2	6.2 ± 0.7	6.9 ± 1.0	16.5	19.3
T3	5.9 ± 0.9	6.4 ± 0.9	14.9	18.9
T4	5.9 ± 0.7	5.8 ± 0.7	14.7	19.0

Table S9: Summary of experimental conditions in the bioturbation and control plots, including total Pd and plastics added, recovery of nanoplastics, final moisture content of soil at sampling point, mean weekly water application and initial bulk density.

			T1	T2	T3	T4	C
Pd per column		*(mg)*			3.9		
Plastics per column		*(mg)*			588		
Mean recovery		*(%)*	64 ± 4	72 ± 2	70 ± 2	71 ± 1	74 ± 5
Mean recovery in L1		*(%)*	58 ± 2	60 ± 3	49 ± 3	48 ± 2	61 ± 7
% of WHC at sampling	layer 1		40 ± 1	41 ± 3	49 ± 2	45 ± 0	42 ± 1
	layer 2		42 ± 2	43 ± 2	46 ± 1	46 ± 3	41 ± 2
	layer 3		40 ± 2	42 ± 2	41 ± 1	42 ± 4	42 ± 2
	layer 4		36 ± 1	36 ± 1	35 ± 1	35 ± 2	36 ± 1
total water applied		*(mm)*					
water per week		*(mm)*	7.7	8.0	8.4	8.3	8.4
application times (total)		*(nbr)*	2	4	7	9	9
Initial bulk density		*(g cm-³)*	1.25 ±0.06	1.22 ±0.03	1.23 ±0.03	1.23 ±0.03	1.24 ±0.03

Table S10: Pd-concentrations detected in the bioturbation plots for all timepoints (T1-T4), all layers (L1-L4) and all replicate plots (rep1-rep3) and all replicate soil subsamples (rep1-1 to rep1-3).

		Plot replicate 1			Plot replicate 2			Plot replicate 3				
		Soil rep 1	Soil rep 2	Soil rep 3	Soil rep 1	Soil rep 2	Soil rep 3	Soil rep 1	Soil rep 2	Soil rep 3		
		Pd (µg kg^{-1})			Pd (µg kg^{-1})			Pd (µg kg^{-1})				
	Layer	rep1-1	rep1-2	rep1-3	rep2-1	rep2-2	rep2-3	rep3-1	rep3-2	rep3-3	**Mean**	**Stdev**
T1	L1	15757	14215	14479	14958	15786	15176	15432	14408	14685	14989	± 586
	L2	383	337	324	1280	1110	915	702	898	838	754	± 346
	L3	39.3	37.3	31.7	61.8	59.0	37.2	-4.1	71.4	66.6	44.5	± 23
	L4	-4.6	-7.8	-5.0	34.0	29.0	18.5	4.9	16.9	-2.1	9.3	± 26
T2	L1	17655	15775	15382	14453	13976	16381	15901	15888	15097	15612	± 1078
	L2	1060	590	610	356	400	395	921	990	683	667	± 268
	L3	125.8	112.3	143.7	92.2	201.8	132.0	223.6	336.8	167.7	170.7	± 75
	L4	27.0	23.6	22.2	32.8	37.1	35.3	48.8	60.0	53.1	37.8	± 13
T3	L1	11238	11859	12316	12837	12881	13509	12301	13218	13978	12682	± 848

	L2	1018	1022	1075	1040	1307	963	1290	973	1204	1099	± 133
	L3	328.3	350.9	324.2	312.2	298.4	246.3	392.9	302.7	328.6	320.5	± 40
	L4	78.3	68.8	50.7	79.3	50.8	109.9	52.5	62.2	61.0	68.2	± 19
T4	L1	13292	12748	12967	11626	13028	12258	12292	11991	12504	12523	± 537
	L2	824	972	966	1471	1225	1235	1150	1386	1103	1148	± 208
	L3	176.6	160.4	154.0	326.3	392.2	326.7	341.2	381.0	347.2	352.4	± 28
	L4	16.3	17.8	20.8	182.3	146.3	127.8	82.5	101.3	104.8	124.2	± 36
C	L1	17239	19985	16038	14383	13842	14437	16560	15430	15793	15967	± 1864
	L2	194	507	103	66	54	51	60	79	35	127	± 150
	L3	-3.1	-3.1	-2.1	-16.8	-2.3	2.2	2.2	2.6	-2.0	-2.5	± 6
	L4	-7.0	-2.6	-6.6	1.5	-3.0	-1.9	1.0	-1.8	0.7	-2.2	± 3

Table S11: Experimental and simulated data of bioturbation plots in mean Pd-concentrations mg kg^{-1} for all timepoints and layers. Model 13A and Model 13B are displayed in Figure 13A and 13B.

	Time (days)	**Measured**	Model 13A	Model 13B
			Pd (mg kg^{-1})	
layer 1	0	26.1*	26.1	26.1
	7	15.0	12.4	16.5
	14	15.6	10.4	13.3
	21	12.7	7.9	11.4
	28	12.5	7.8	10.1
layer 2	7	0.754	6.232	4.705
	14	0.667	6.367	5.921
	21	1.099	5.974	6.281
	28	1.148	5.925	6.322
layer 3	7	0.044	0.267	0.023
	14	0.171	0.657	0.207
	21	0.321	1.375	0.466
	28	0.352	1.364	0.728
layer 4	7	0.009	0.000	0.000
	14	0.038	0.000	0.000
	21	0.068	0.002	0.000
	28	0.124	0.032	0.000

*Note: expected spike concentration at T=0, not measured.

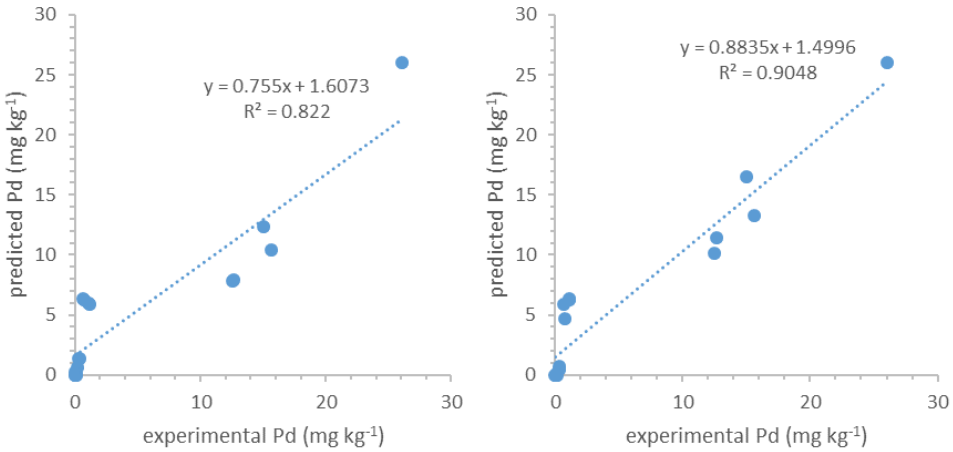

Figure S3: Fit of the bioturbation model, expressed as R² of the regression of simulated versus observed data for models displayed in Figure 13A (left) and 13B (right).